1.0

2.8   2.5
3.2   2.2

2.0

1.1

1.8

1.25 1.4 1.6

MICROCOPY RESOLUTION TEST CHART

NAVAL POSTGRADUATE SCHOOL
Monterey, California

THESIS

AN INVESTIGATION OF PLASMA - SURFACE
INTERACTIONS ON SELECTED
CONDUCTORS AND INSULATORS.

by

Joseph Henry Barker III
and
Robert Jacque Rush

December 1980

Thesis Advisors: F. Schwirzke
                    K. D. Challenger

REPORT DOCUMENTATION PAGE	READ INSTRUCTIONS BEFORE COMPLETING FORM

1. REPORT NUMBER	2. GOVT ACCESSION NO. AD-A098089	3. RECIPIENT'S CATALOG NUMBER

4. TITLE (and Subtitle)	5. TYPE OF REPORT & PERIOD COVERED
AN INVESTIGATION OF PLASMA - SURFACE INTERACTIONS ON SELECTED CONDUCTORS AND INSULATORS	Master's Thesis: December 1980
	6. PERFORMING ORG. REPORT NUMBER

7. AUTHOR(s)	8. CONTRACT OR GRANT NUMBER(s)
Joseph Henry Barker III and Robert Jacque Rush	

9. PERFORMING ORGANIZATION NAME AND ADDRESS	10. PROGRAM ELEMENT, PROJECT, TASK AREA & WORK UNIT NUMBERS
Naval Postgraduate School Monterey, California 93940	

11. CONTROLLING OFFICE NAME AND ADDRESS	12. REPORT DATE
Naval Postgraduate School Monterey, California 93940	December 1980
	13. NUMBER OF PAGES 107

14. MONITORING AGENCY NAME & ADDRESS(if different from Controlling Office)	15. SECURITY CLASS. (of this report)
Naval Postgraduate School Monterey, California 93940	Unclassified
	15a. DECLASSIFICATION/DOWNGRADING SCHEDULE

16. DISTRIBUTION STATEMENT (of this Report)

Approved for public release; distribution unlimited

17. DISTRIBUTION STATEMENT (of the abstract entered in Block 20, if different from Report)

18. SUPPLEMENTARY NOTES

19. KEY WORDS (Continue on reverse side if necessary and identify by block number)

Unipolar Arcs, Plasma Surface Damage, Unipolar Arcing Damage Mechanisms, Laser-Target Damage Mechanism

20. ABSTRACT (Continue on reverse side if necessary and identify by block number)

Damage caused by plasma-surface interactions is of concern in fields involving the use of such plasma devices as particle beam weapons, high power lasers and controlled thermonuclear fusion reactors. Several conductors and non-conductors were exposed to a plasma to study the plasma-surface interaction damage.

In one part of the study, the plasma was induced by irradiating the surface of the samples with a Q-switched neodymium laser. Some

DD, FORM 1473 EDITION OF 1 NOV 65 IS OBSOLETE
S/N 0102-014-6601 |

Block 20 Cont'd:

of the samples were irradiated in air, at atmospheric pressure,
and in a vacuum, to compare the difference in the extent of the
damage on the same types of samples at different pressures. In
the other part of the study, several titanium coated conductors
and titanium coated non-conductors were exposed to the plasma of
a tokamak.
    Both the metal conductors in the first part of the study,
and the titanium coatings in the second part of the study, were
damaged by unipolar arcing. Nickel showed less evidence of uni-
polar arcing damage than any of the other samples studied.

An Investigation of Plasma-Surface
Interactions on Selected
Conductors and Insulators

by

Joseph Henry Barker III
Lieutenant Commander, United States Navy
B. S., United States Navy Academy, 1967

and

Robert Jacque Rush
Lieutenant Commander, United States Navy
B. S., Prairie View A&M College, 1972

Submitted in partial fulfillment of the
requirements for the degree of

Master of Science in Physics
(Joseph Henry Barker III)

Master of Science in Engineering Science
(Robert Jacque Rush)

from the
NAVAL POSTGRADUATE SCHOOL
December 1980

Author: _____

Author: _____

Approved by: _____
                                    Thesis Advisor

             _____
                                    Second Reader

             _____
Chairman, Department of Physics and Chemistry

             _____
                    Dean of Science and Engineering

3

ABSTRACT

Damage caused by plasma-surface interactions is of concern in fields involving the use of such plasma devices as particle beam weapons, high power lasers and controlled thermonuclear fusion reactors. Several conductors and non-conductors were exposed to a plasma to study the plasma-surface interaction damage.

In one part of the study, the plasma was induced by irradiating the surface of the samples with a Q-switched neodymium laser. Some of the samples were irradiated in air, at atmospheric pressure, and in a vacuum, to compare the difference in the extend of the damage on the same types of samples at different pressures. In the other part of the study, several titanium coated conductors and titanium coated non-conductors were exposed to the plasma of a tokamak.

Both the metal conductors in the first part of the study, and the titanium coatings in the second part of the study, were damaged by unipolar arcing. Nickel showed less evidence of unipolar arcing damage than any of the other samples studied.

TABLE OF CONTENTS

5

ACKNOWLEDGEMENTS

We are particularly grateful for the advice, help and support of Robert Sanders and Tom Kellog. Robert Sanders cheerfully supported our work in the neodymium-glass laser laboratory and helped to obtain the materials which made this research possible. Tom Kellog's support in the material science laboratories was invaluable. His advice on target preparation plus the many hours he spent aiding us with the electron microscope are deeply appreciated.

Most of all, we would like to thank Professors F. Schwirzke and K. D. Challenger for their help and guidance throughout this thesis. Without their concern and interest this research would not have been possible.

Lieutenant Commander Bob Rush adds: "Most of all, I would like to thank my wife Mary and my children Stephanie and Robert Jr. whose love, cooperation and encouragement helped me make it through this whole educational venture."

I. INTRODUCTION

The rising cost of fossil fuels has spurred the development of alternative energy sources. Two of the more promising new energy sources are magnetically confined fusion and laser light initiated fusion. Fusion by magnetic confinement works by confining a plasma with a strong magnetic field while heating the plasma to the fusion ignition temperature. Fusion with laser light uses inertial confinement while heating matter to very high temperatures thereby initiating a controlled thermonuclear reaction. Although, the theory is promising, the actual engineering to achieve a controlled thermonuclear reaction using magnetic confinement or laser light is very challenging.

One of the most difficult engineering aspects of the problem is to prevent damage to the reactor wall in the presence of fusion products and a hot plasma. This thesis investigated how different materials behaved in the presence of a laser generated plasma.

Plasma generated damage to a reactor wall has two undesirable results. First, and most obvious, is that the containment vessel will gradually erode by the interaction of a plasma with the wall. The second undesirable result is that the plasma becomes contaminated with high-Z wall materials. These impurities prevent the plasma from achieving ignition temperature

10

and ultimately prevent the thermonuclear reaction from occuring. Since high energy fusion products are also present during this reaction, the challenge is to choose low-Z materials which will resist both damage by the plasma and the fusion products.

There are several other applications where plasma-surface interactions are important. Both high energy lasers and beam weapons operate under plasma conditions. Preventing self-damage to these devices is a major engineering challenge. In addition, when a laser is used as a weapon, the initial inter-action of the laser light with the target generates a plasma at the target which then shields the target from further direct damage by the laser light. In this case, the problem is to enhance the coupling of laser energy with the target.

There are three major damage mechanisms when a hot plasma is in contact with a solid. These damage mechanisms are evaporation, sputtering and unipolar arcing.

Evaporation occurs when radiant heat and plasma energy is absorbed by the wall surface and the surface temperature in-creases the vapor pressure. When a neutral atom or ion imparts enough energy to a wall surface atom so that the binding energy of the wall surface atom is exceeded, sputtering results. Unipolar arcing occurs when a hot dense plasma and a conduct-ing wall interact. An electrical arc is established between the wall and the plasma with the wall acting as both the cathode and anode.

11

Various surface studies of conductors have indicated that unipolar arcing is a significant plasma-surface interaction damage mechanism. Insulators have not been studied as extensively as conductors.

Lautrop and Keville [1] investigated the effectiveness of thin films of titanium carbide on stainless steel to inhibit damage by unipolar arcing. They concluded that a titanium carbide coating on stainless steel could be a solution to the unipolar arcing problem.

In this thesis, a comparative study of plasma-surface interactions with uncoated metals and coated insulators was made. The samples that were studied included uncoated stainless steels, pure nickel, copper, titanium, tin, tungsten carbide coated with titanium, and stainless steel coated with titanium.

A comparison was made between the tested samples to discover if a specific property or properties of the tested samples is responsible for reducing or inhibiting unipolar arcing. The properties of the materials that were considered during this study were melting temperature, electrical and thermal conductivity, crystal structure and ionization energy.

II. BACKGROUND AND THEORY

A. LASER LIGHT PLASMA GENERATION

1. Introduction

A laser is capable of producing extremely high power coherent light. Whenever high power coherent light is incident upon any material, the light interacts with the material. A portion of the light is reflected and the remainder is absorbed and converted to thermal or mechanical energy which propagates into the material. If the power is high enough, the material interacts with the incident light energy by melting and vaporizing. Once the material has begun to vaporize and the laser provides a sufficient amount of energy, ionization of the vapor plume occurs forming a plasma above the material's surface. As the plasma is formed, it expands away from the material's face and propagates across the face while interacting with the material's surface.

2. Laser Light Coupling with a Material

As laser light falls upon a material, a portion of the light is reflected and the remainder of the energy is absorbed by conduction band electrons. The energy of the conduction band electrons is raised. Collisions transfer this energy throughout the solid thereby raising the solid's temperature.

The amount of energy that is absorbed by the material is governed by the reflectivity of the material. Reference 2

13

gives the reflectivity as:

$$R = \frac{(n - 1)^2 + k^2}{(n + 1)^2 + k^2}$$ 2-1

where the light is normal incident to the material and the material's interface is in a vacuum. The factor (k) is the extinction coefficient and (n) is the material's index of refraction. The reflectivity, R, was found to depend upon the frequency of the laser (ω), the constant (m*/N) and the dc conductivity (d). Thus $R = f(\omega, m*/N, d)$ where:

N = electron concentration (number of electrons per unit volume)

m* = electron effective mass .

As the temperature of the target surface rises, the optical characteristics of the target material change causing a decrease in the reflectivity and consequently a greater amount of the laser energy is absorbed [3]. This continues until the target material starts to melt. Experiments have shown that at the melting point, there is a marked increase in the rate at which laser light energy is absorbed [4].

3. Thermal and Mechanical Propagation of Energy into the Material

When a laser pulse strikes a target, the surface temperature is rapidly raised to a high value. The temperature just a few microns below the surface may reach only about one tenth of the surface temperature [5]. This creates

14

extremely large temperature gradients between the surface and the immediate substrate causing a thermal and mechanical shock wave to propagate into the target. Lasers have many useful applications at power levels which cause melting of the target but are not high enough to cause plasma formation. Some of these applications are laser welding and laser surgery.

Understanding this stage of the interaction requires an understanding of the heat flow within the target material. The heat flow equation [6] is:

$$DC \frac{\partial T}{\partial t} = \frac{\partial}{\partial x} Q\left(\frac{\partial T}{\partial x}\right) + \frac{\partial}{\partial y} \left(Q\frac{\partial T}{\partial y}\right) + \frac{\partial}{\partial z} \left(Q\frac{\partial T}{\partial z}\right) + A \qquad 2-2$$

where
      D = density of the material

      C = specific heat

      T = temperature

      t = time

      Q = thermal conductivity .

The quantity (A) is a characteristic of the laser and is the heat produced per unit volume per unit time. The quantity (A) must be known to calculate the heat flow, but it is very difficult to establish its value in an actual laser-material interaction.

As the target's temperature rises, the vaporization point will be reached. The boiling point of the target is pressure dependent. During a laser-material interaction the actual

15

boiling point is difficult to determine because of the con-
current effects of the laser upon the target surface.

Experiments have shown that the radiation pressure exerted
by a laser beam on a target can be extremely great. Hughes
writes in References 6 "for example, a pulse of 100 MW peak
power absorbed is an area of 10^{-4} cm^2 exerts a peak pressure
of 300 atmospheres. When evaporation is taking place, even
greater pressures arise due to the recoil on the surface from
departing particles." The pressure caused by recoil can be as
much as 10^4 times as great as the pressure of the incident
radiation. This pressure is given [8] by:

$$P = \frac{F \sqrt{GT_v/M}}{L_v + CT_v} \qquad\qquad 2-3$$

where: G = gas constant

T_v = vaporization temperature

M = molecular weight

L_v = latent heat of vaporization

C = specific heat of the material

F = absorbed power density in watts/cm^2

Although the time that it takes to start melting the
target is important in some laser applications, for high
power lasers the liquid phase has very little significance as
a step towards plasma formation. Once vaporized material that
is blown off the target begins to absorb laser radiation,
plasma production begins.

16

4. Plasma Production

The temperature of the vapor above the target surface continues to rise as long as the rate of absorption of energy from the laser is great enough to overcome cooling caused by expansion and conduction. A significant number of atoms will be ionized by collisions when the vapor reaches a high enough temperature [7]. The electrons within the vapor plume absorb the laser's light energy.

When the vapor plume reaches the plasma state, the free-free transitions of electrons colliding with positive ions causes strong absorption of the laser light and the high plasma density shields the surface of the target from further direct laser beam interaction. "The presence of even a small proportion of free electons causes a marked increase in the absorption coefficient of a gas, and hence an increase in the rate of heating, leading to a greater degree of ionization, and so on. Electron-ion absorption becomes the dominant heating process."[7]

When the electron density reaches a critical value, the laser beam decouples from the target surface. The critical density occurs when the laser frequency equals the plasma frequency such that $\omega = \omega_p$ and is given by

$$n_c = m\omega^2/4\pi e^2 \qquad\qquad 2\text{-}4$$

where: n_c = critical density

 m = electron mass

17

ω = laser frequency

e = electron charge .

The laser's energy is expended on heating the hot plasma above the target surface. As full ionization is approached and $n > n_c$ however, the power absorbed per particle becomes density dependent and starts to fall.

This leads to a self-regulating mechanism for plasma density. When the laser light strikes the target, a vapor plume is formed and is ionized. The ionized vapor shields the target from the laser light causing a decrease in vapor production. This reduces the amount of shielding and the laser light again reacts with the surface starting the process over.

The hot plasma plume initially expands rapidly in the direction of the light source and exerts a plasma pressure upon the target surface. The plasma pressure is defined [9] by:

$$p = nKT \qquad\qquad 2\text{-}5$$

where: n = plasma density

K = Boltzmann's Constant

T = plasma temperature .

For an neodymium laser produced plasma with $n = 10^{21}$ particles/cm^3 and KT = 100 ev, the plasma pressure is 1.83 X 10^5 atmospheres.

The hot dense plasma expands from the focal spot across the target surface. The mean thermal velocity of expansion of the plasma [10] is:

18

$$V^2 = \frac{(n_e + n_i)\ KT}{n} \qquad\qquad 2\text{-}6$$

where: n_3 = number of electrons

n_i = number of ions

n = plasma density

B. ENGINEERING DIFFICULTIES CAUSED BY PLASMA-SURFACE INTERACTIONS

When a hot plasma is in contact with or adjacent to a conducting or nonconducting material, the plasma interacts with the material. This interaction can have two undesirable consequences: the plasma can damage the surface of the material and the plasma may become polluted by the material's atoms.

1. Surface Damage

The plasma causes three kinds of surface erosion: sputtering, evaporation and unipolar arcing. Once the smooth surface of a material is initially damaged, the rate of further damage is enhanced.

2. Plasma Pollution

Plasma pollution is an important problem that must be overcome to achieve sustained, magnetically confined fusion. Plasma-surface interaction products contaminate the plasma resulting in radiation losses from high atomic number Z particles. This cools the plasma sufficiently so that the plasma can not be sustained at fusion temperatures [11].

3. Plasma-Surface Interaction Damage Mechanisms

    a. Evaporation

    When a material absorbs enough radiant heat and
plasma energy, melting followed by evaporization results. If
the surface temperature as a function of time and the equi-
librium vapor pressures curves of the material are known,
evaporization can be predicted accurately. Since all plasmas
are very hot, evaporation in the presence of a dense plasma
is a major problem.

    b. Sputtering

    Because of the high temperatures of a plasma, the
ions have a great amount of energy. When a high energy ion
collides with a material's surface, a collision cascade with
the lattice atoms results [12]. Sputtering occurs when the
collision cascade imparts enough energy to a surface atom so
that the surface atom's binding energy is exceeded.

    c. Unipolar Arcing

    Both evaporation and sputtering are enhanced in
the presence of unipolar arcing. Unipolar arcing has been
reported as the most significant of the three damage
mechanisms [13].

    Unipolar arcing occurs when an electrical arc is
established between the surface of a material and a hot dense
plasma. This causes cratering of the material's surface and
results in severe plasma pollution.

Because a plasma is a quasi-neutral gas of charged particles exhibiting collective behavior, it has a fundamental characteristic of being able to shield out electric potentials applied to it. The Deby length (L_D) is the characteristic shielding length of the plasma and is given by:

$$L_D = \left[\frac{K\,T_e}{4\pi n\,e^2} \right]^{1/2} \qquad\qquad 2\text{-}7$$

where: T_e = electron temperature

n = plasma density

e = electron charge .

Since the ions and electrons have different masses, the electrons will have much larger thermal velocities than the ions. Therefore, the electrons will tend to leak from the plasma to the containment wall much more rapidly than the ions. This causes the plasma to take on a positive potential relative to the wall.

A sheath is formed at the perimeter of the plasma between the plasma and the adjacent wall. This sheath establishes a potential barrier to the electrons. This potential is great enough to equalize the ion and electron losses.

If the sheath potential becomes large enough to sustain an arc, unipolar arcing occurs. Electrons are emitted from a surface spot into the plasma. The adjacent potential is reduced allowing electrons from the plasma to reach the wall, thereby closing the current loop [14].

21

4. Damage Prevention

There are two areas being studied to reduce damage by plasma-surface interactions. The first approach, which is particularly applicable to avoid damage to the components of high energy lasers, is to prevent the surface breakdown process which results in surface damage. The second area of study is to find materials which can resist plasma induced damage.

a. Lasers

The optical components of high energy lasers are especially vulnerable to surface damage. Any imperfection in the optical train of a laser tends to cause the laser light to self-focus within the optical element [15]. If this self-focusing occurs near the surface of the material, it can rapidly lead to breakdown and surface damage of the optical element [16]. If the surface damage progresses, evaporation and plasma formation can result.

Experiments have shown that the surface damage mechanisms are enhanced when the surface layer of the optical elements contain imperfections, inclusions, microcracks, or contaminated materials [17]. Therefore, the emphasis on preventing surface damage to optical elements and hence plasma formation has been concentrated on eliminating surface imperfections. Also, the laser's power must be carefully controlled so as not to exceed damage thresholds.

Most of the methods used to protect the optical elements of a laser involve some sort of a super-polishing

22

technique. These methods involve bowl-feed polishing, ion-beam polishing, laser polishing, (plasma conditioning), and chemical etching [18]. All of these polishing techniques remove the surface layer of the optical elements along with the inherent imperfections.

b. Other Devices

In other devices, prevention of plasma formation may not be possible or desirable. Fusion reactors, for example, require the presence of plasmas to operate. Therefore, the major effort is concentrated upon finding materials or combination of materials which can resist plasma induced damage.

One of the more promising techniques for controlling plasma-surface interactions is coating materials with substances that resist plasma damage. Lautrup and Keville [1] found that TiC coated stainless steel could be useful in controlling unipolar arcing. Coatings probably work because they can make the surface adjacent to the plasma smooth and free of inclusions, microvoids and impurities.

III. EXPERIMENTAL DESIGN

A. EQUIPMENT

The equipment used to study plasma-surface interactions consisted of a neodymium-glass laser and a target test chamber. Both the laser and the test chamber are shown in Figure 1. The target test chamber was operated both in a vacuum and at atmospheric pressure. A scanning electron microscope equipped with an energy dispersive x-ray analyzer and an optical microscope were used to study the samples. Figure 2 is a schematic diagram of the laser and the target test chamber.

The neodymium-glass laser was used to irradiate the targets mounted in the test chamber. The targets were then studied using both the optical and scanning electron microscope to determine the extent and nature of the plasma-surface interaction.

1. Laser

A KORAD K-1500 neodymium-glass laser was used to illuminate the test targets. The 1.06 μm wavelength laser was operated in the Q-switched mode to achieve pulse widths of about 25 nanoseconds. A detailed description of the laser installation is given by Davis [19].

The laser's output energy can be varied from 0.2 to 15 joules. For this experiment, the laser was operated at an output of 8-12 joules. The laser beam was passed through a
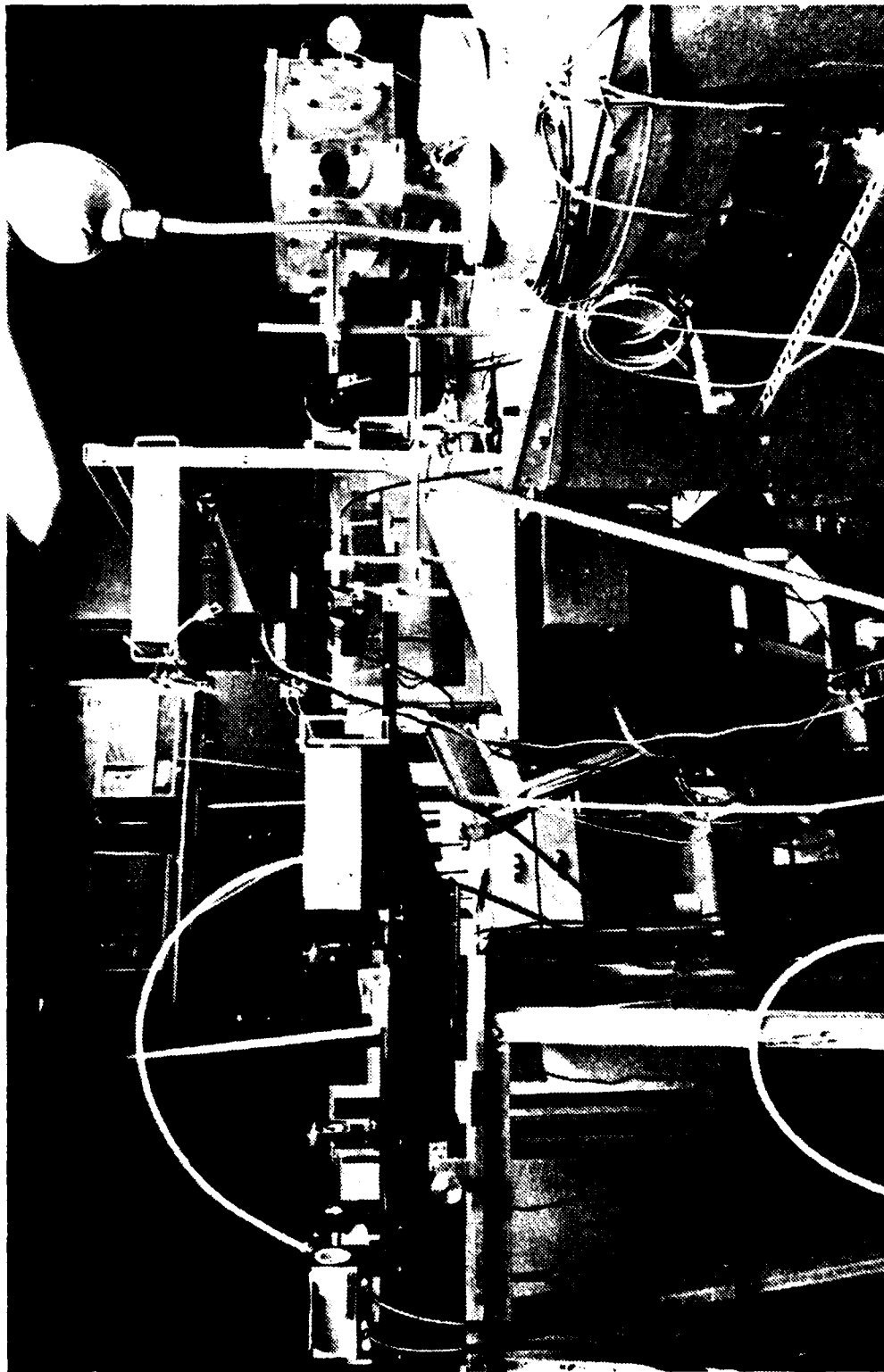
24

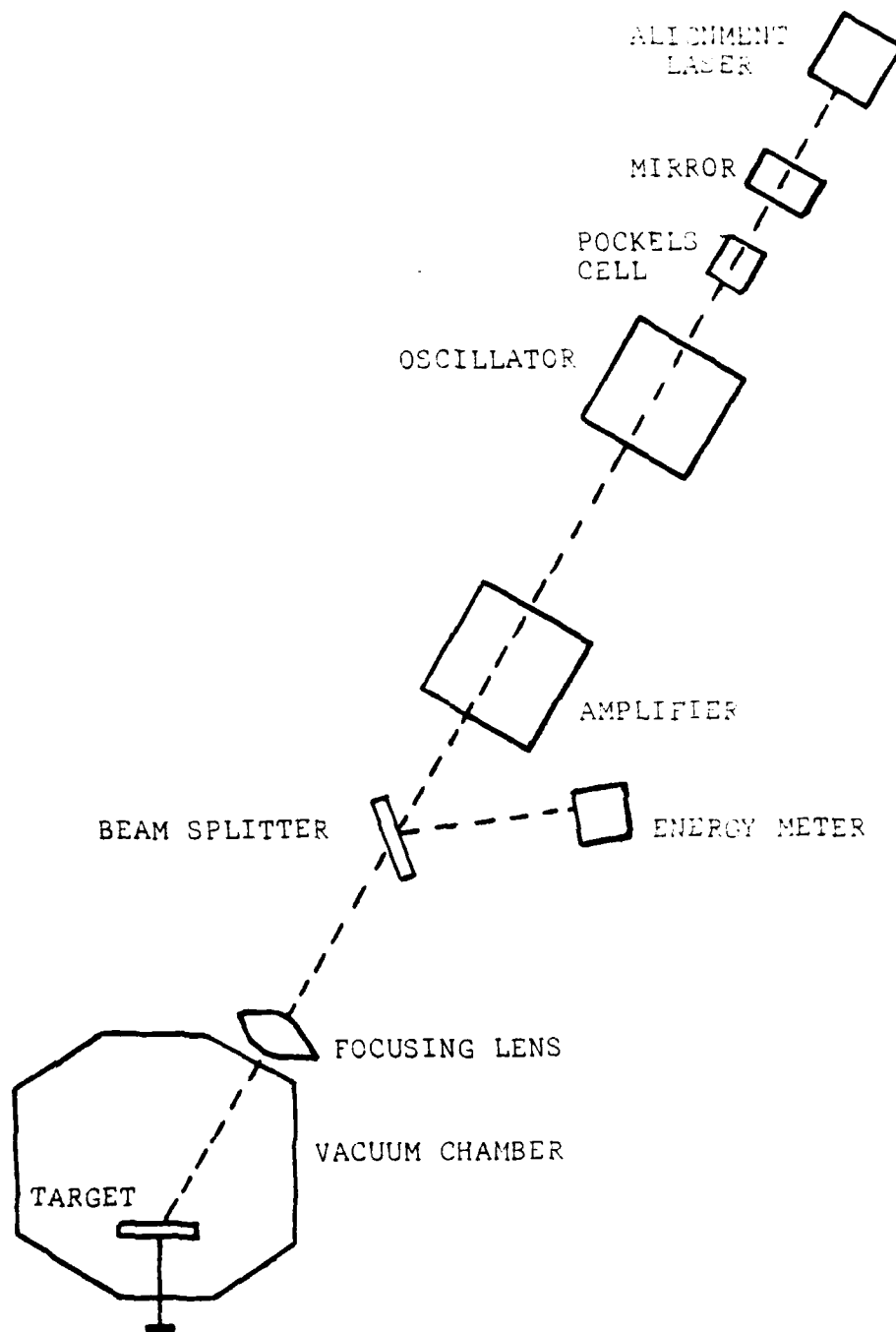FIGURE 1. NEODYMIUM-GLASS LASER AND TARGET TEST CHAMBER.

25

FIGURE 2. LASER AND TEST CHAMBER ARRANGEMENT.

26

twenty-five percent transmission filter to reduce the energy at the target to 2-4 joules. The laser's output energy was measured by a Laser Precision RK-3200 Series Pyroelectric Energy Meter.

2. Target Test Chamber

The target test chamber is a 6 inch cube of baked aluminum which could be evacuated to a pressure of about 10^{-6} torr. The test chamber, seen in Figure 3, is fully described by Lautrup and Keville [1].

3. Optical Microscope

The target surfaces were studied and photographed using a Bausch and Lomb Balpan stereoscope microscope.

4. Scanning Electron Microscope

A Cambridge Stereoscan S4-10 scanning electron microscope was used to study the target surface before and after target irradiation. The microscope uses secondary electrons to form images. Figure 4 is a schematic diagram of this microscope.

B. TARGETS

This experiment extended the work of Lautrup and Keville [18] who examined plasma-surface interactions on TiC coated stainless steels. This study investigated plasma-surface interactions with other materials, conductors and nonconductors.
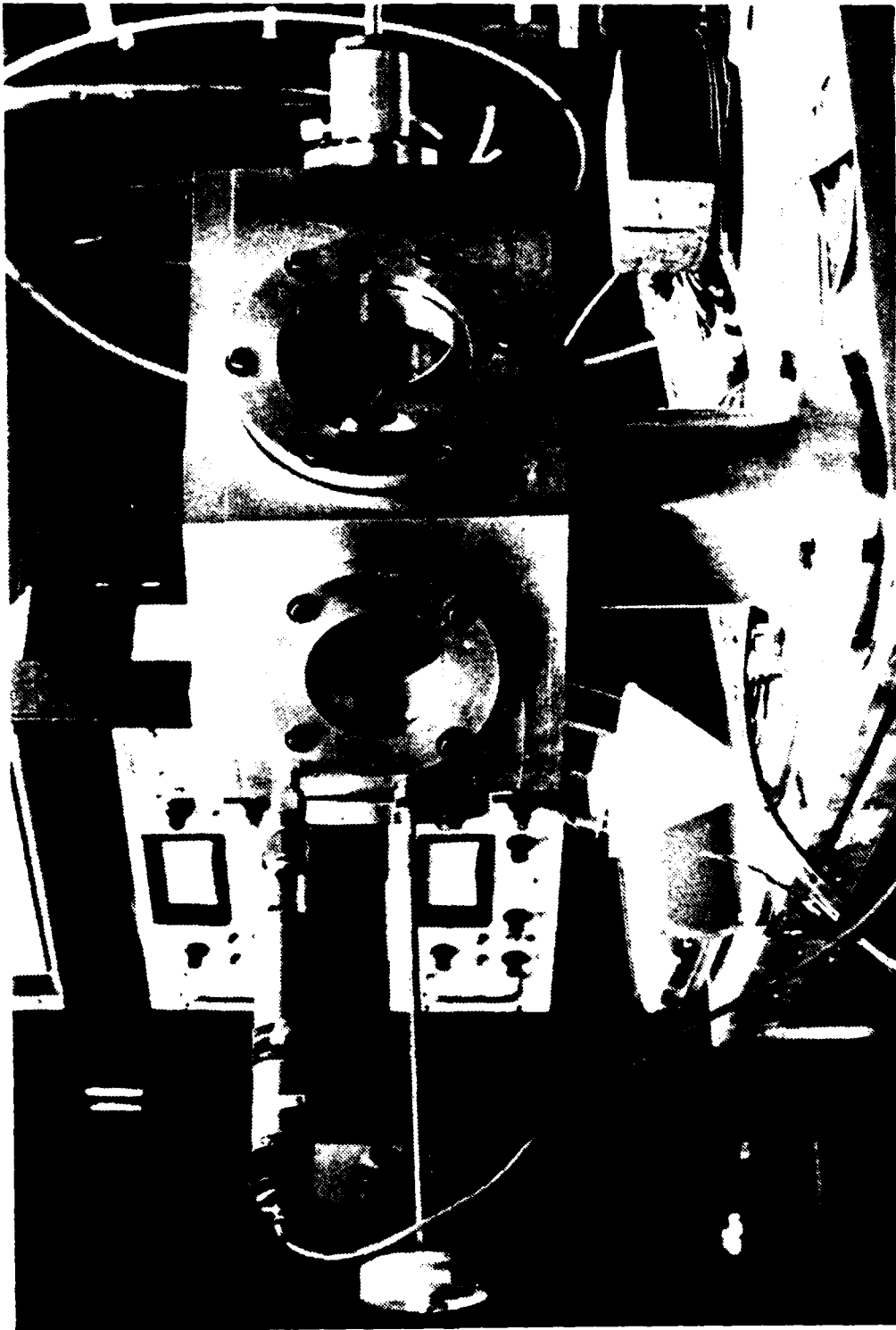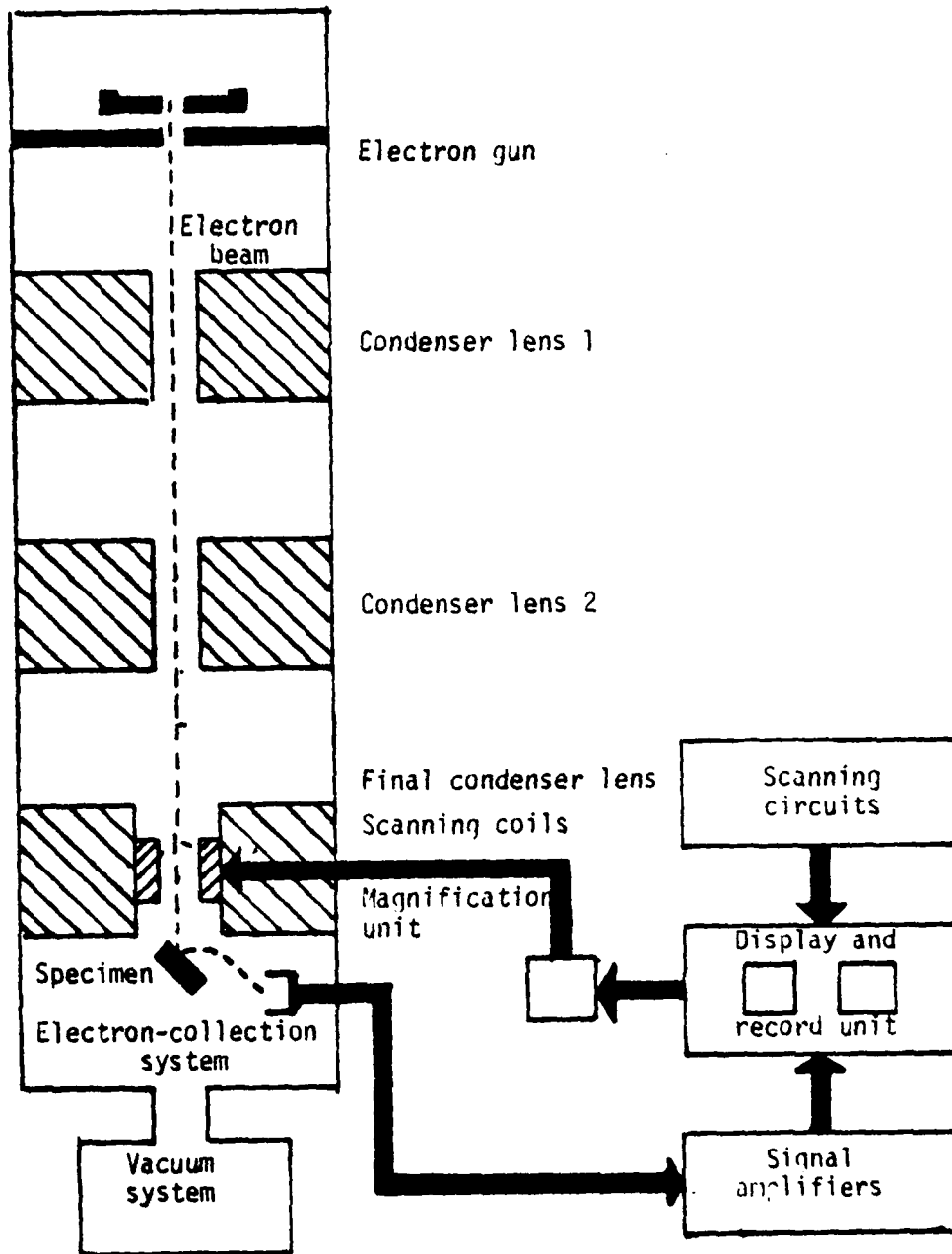
FIGURE 3. TARGET TEST CHAMBER.

Electron gun

Electron beam

Condenser lens 1

Condenser lens 2

Final condenser lens
Scanning coils

Magnification unit

Specimen

Electron-collection system

Vacuum system

Scanning circuits

Display and record unit

Signal amplifiers

FIGURE 4.   SCANNING ELECTRON MICROSCOPE.

29

1. Conducting Targets

The following conducting targets were investigated:
(1) uncoated type 304 stainless steel, (2) nickel, (3) copper,
(4) tin, (5) tungsten carbide, and (6) titanium coated stainless steel.

a. Preparation of Conducting Targets

The surfaces of the metallic conducting targets were polished using standard metallurgical techniques. Reference 20 describes these polishing methods.

Polishing is designed to reduce surface irregularities that tend to promote arcing on the surface of the target as described by Lautrup and Keville [1]. These irregularities can be in the form of whisker-like surface projections or dielectric spots. The whiskers establish strong local fields and provide a near plasma point that can be easily heated by ion bombardment. Dielectric spots are metal oxides or surface contamination such as oil and water films. These surface areas charge up to promote arcing.

2. Nonconducting Samples

The nonconducting samples consisted of three glass plates that had been exposed to a plasma and were provided for this study by The Center for the Study of Plasma Physics and Fusion Engineering at UCLA and the Air Force Weapons Laboratory at Albuquerque, New Mexico.

Sample number one was an antenna shield from the UCLA Macrotor tokamak. This shield consisted of one-half of a glass tube 4 centimeters in diameter and 29 centimeters long. This tube was coated with a thin titanium film. Figure 5 is a photograph of this tube.

Sample number two was the 6.2 centimeter square window of an Air Force CO2 laser. A photograph of the tube is shown in Figure 6.

Sample number three was a 4 centimeter glass tube that had a thin film coating of titanium applied to it by a plasma process. This sample is shown in Figure 7.

C. TESTING PROCEDURES

1. Conducting Targets

Each laser target was cleaned with acetone, mounted and placed in the test chamber. Most of the tests were conducted with a vacuum of 10^{-6} torr. Three samples were radiated with the laser at atmospheric pressure.

After the target was properly aligned in the test chamber, the neodymium laser was fired at the target. The energy incident on the targets varied from 2 to 4 joules for a duration of 25 to 30 nanoseconds. The focused energy provided by the laser was measured by reflecting eight percent of the total energy to the power meter.

The laser power was sufficient to cause breakdown of the target material and the formation of a hot plasma above
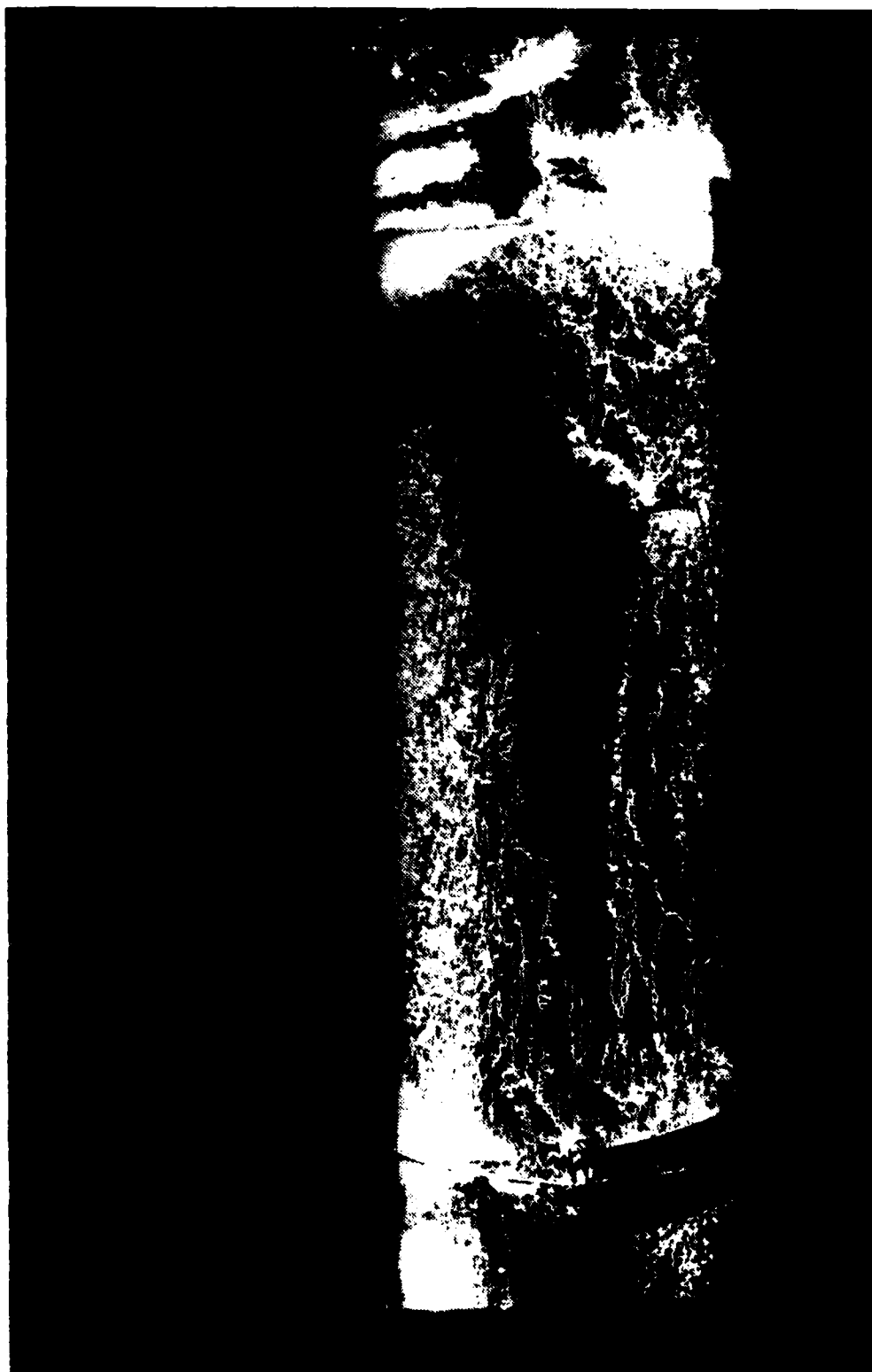
FIGURE 5. NONCONDUCTING SAMPLE NUMBER ONE IS AN ANTENNA SHIELD FROM THE UCLA MACROTOR TOKAMAK. THIS TUBE HAS A GLASS SUBSTRATE COATED WITH TITANIUM. THE TITANIUM COATING IS BLACK. THE WHITE AREAS ARE ARC TRACKS CAUSED BY PLASMA-SURFACE INTERACTIONS.
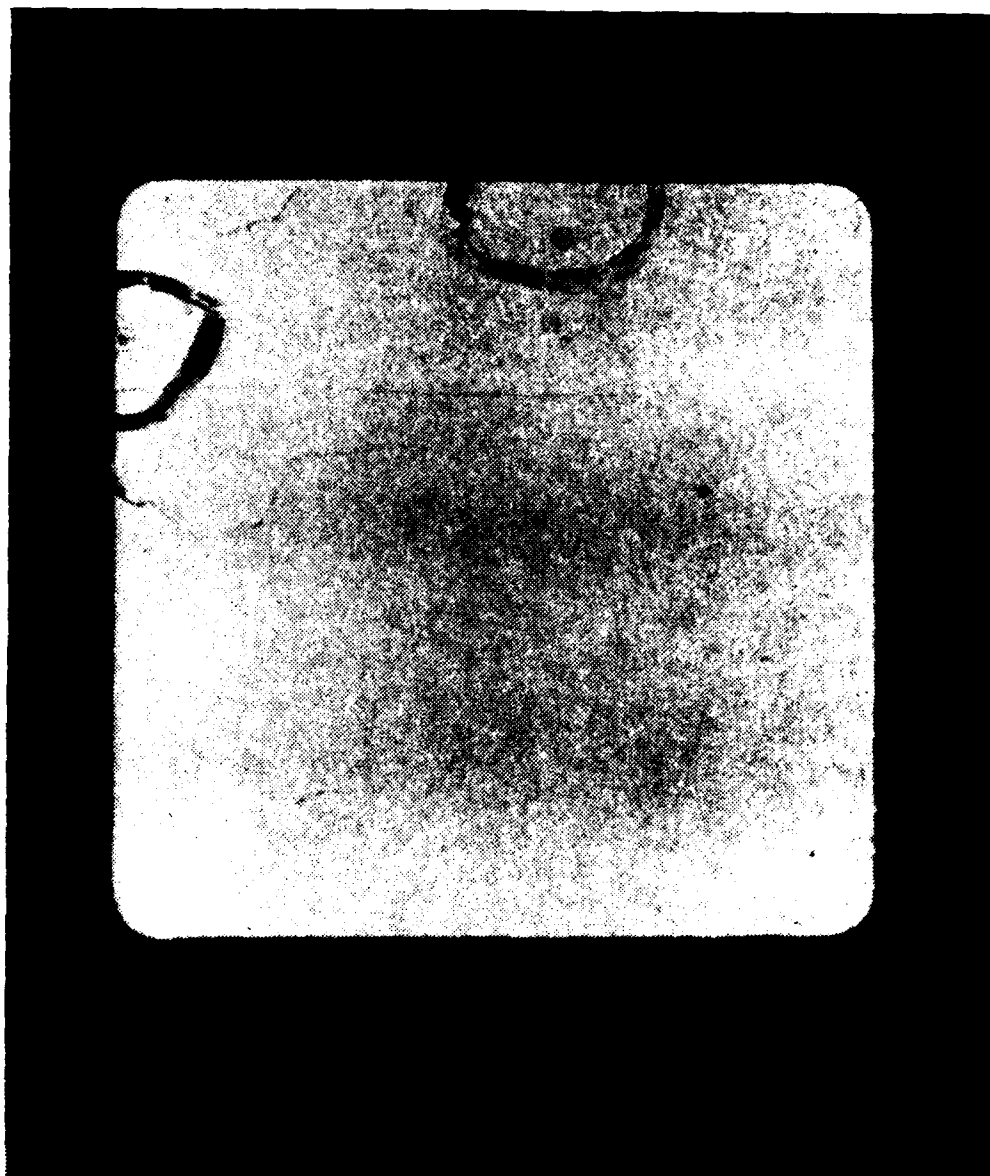
FIGURE 6. NONCONDUCTING SAMPLE NUMBER TWO IS A 6.2 CENTIMETER SQUARE
WINDOW OF AN AIR FORCE CO_2 LASER. THE CIRCULAR AREAS ARE
DAMAGE CAUSED BY PLASMA-SURFACE INTERACTIONS. (1.5X)

33

Grey colored half of titanium coated tube.

Black colored half of titanium coated tube.

FIGURE 7. NONCONDUCTING SAMPLE NUMBER THREE IS A UNTREATED ALUMINA TUBE THAT HAD A THIN FILM COATING OF TITANIUM APPLIED BY THE PLASMA PROCESS. (1.5X)

the target's surface. A post test examination of each target was conducted using the Bausch and Lomb Stereomicroscope and scanning electron microscope (SEM) to determine the nature of the plasma-surface interaction.

The depth of the craters was determined by using the optical microscope. The optical microscope was focused on the target surface and then refocused on the bottom of the crater. The difference in the focal distances is the crater depth. The surface roughness of the samples was not measured.

2. Nonconducting Samples

The insulator samples were studied with the stereomicroscope and the SEM to determine the extent of the surface damage. The damage to the insulators was compared to the surface interactions of the conductors to determine if insulators might be less prone to damage in the presence of a plasma.

IV. EXPERIMENTAL RESULTS

A. CONDUCTORS

1. Uncoated Stainless Steel

a. Uncoated Stainless Steel Irradiated in a Vacuum

A 0.375 mm thick sheet of type 304 stainless steel was used for this experiment. It was prepared in accordance with standard polishing techniques [20]. The stainless steel was irradiated by the laser operating in the Q-switched mode with 3 to 4 joules of energy.

The main crater of the sample was 60 to 70 μm deep at the center and 1.27 mm in diameter. Figure 8 is a photograph taken by the optical microscope of the outer perimeter of the damaged area at a magnification of 100X. The laser impact area, marked by a large crater, is at the lower left corner of the photograph. Figure 9 is a scanning electron microscope (SEM) view of the main crater. The many dimpled areas that are around the main crater are probably caused by unipolar arcing. The larger dimples were caused by the first arcs while the smaller dimples were formed just before the plasma dissipated. Figure 10 is a picture of the outer perimeter of the same damaged area. The nearly circular craters are again caused by unipolar arcing. The debris in the center of some of the craters was not caused by the plasma-surface interaction. The debris is probably a collection of dust
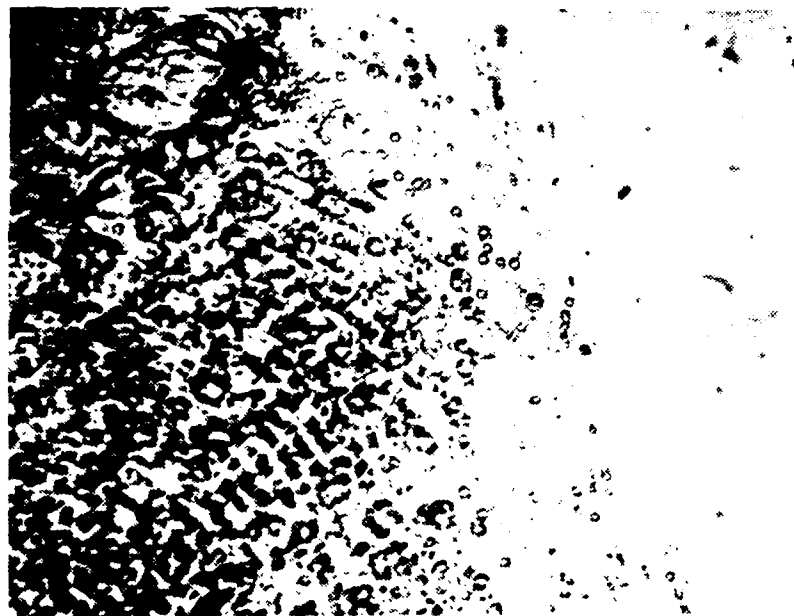
FIGURE 8. UNCOATED STAINLESS STEEL IRRADIATED IN A VACUUM SHOWING CRATER
AT LEFT. THE DAMAGED AREA IS 10 μm DEEP AND .127 mm IN DIAMETER.
(100X OPTICAL MICROSCOPE)

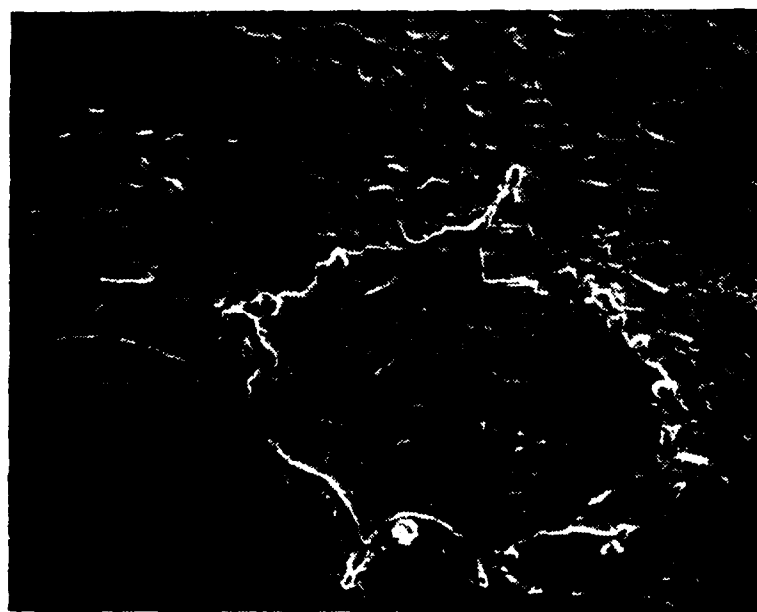FIGURE 9. UNCOATED STAINLESS STEEL CENTRAL CREATER IRRADIATED IN A VACUUM.
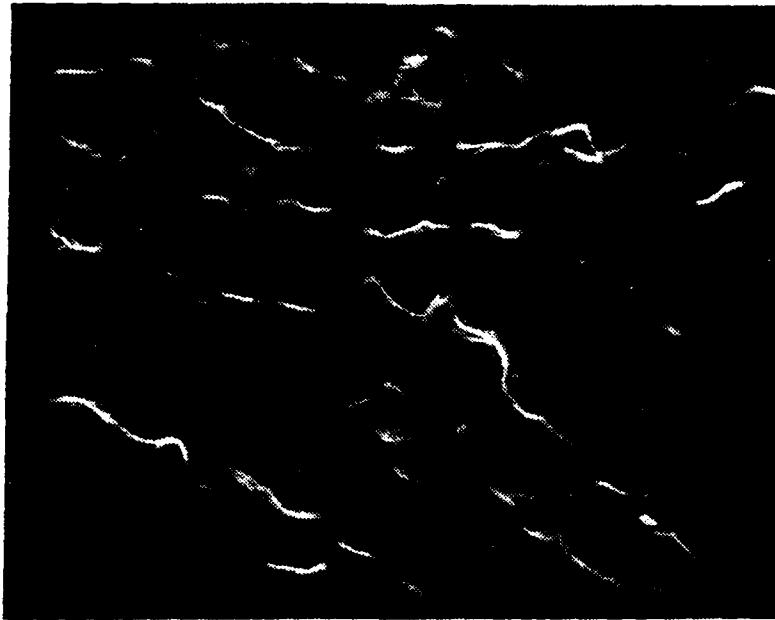THE DIMPLED AREAS ARE CAUSED BY UNIPOLAR ARCS.
(200X SEM)

37

FIGURE 10. VACUUM IRRADIATED STAINLESS STEEL. THIS VIEW IS A MAGNIFICA-
TION OF THE OUTER PERIMETER OF THE CRATER SHOWN IN FIGURE 9.
(500X SEM)

particles and oxidation that occured after the sample was

exposed to the plasma. Figure 11 is a magnification of the

center of Figure 10.

Figures 12 to 14 are photographs of a laser inter-

action with a different area of the same sample. Figure 12

was taken near the center of the new damaged area. Figure 13

is a closer view of the bubble-like areas shown in Figure 12.

The bubbles are caused by the melting of the metal followed

by rapid cooling as molten steel was moving away from the

laser damaged center. Figure 14 shows the outer perimeter of

the damaged area. The main crater is to the right. There is

an abrupt end to the area with large craters. To the left of

the photograph several smaller craters can be seen. The size

38
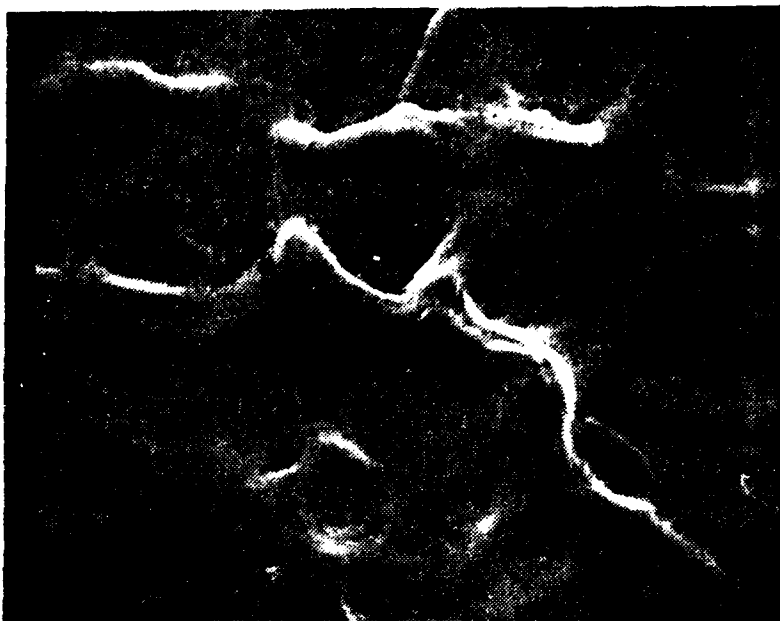
FIGURE 11. VACUUM IRRADIATED STAINLESS STEEL. THIS VIEW IS AN ENLARGE-
MENT OF CENTER OF FIGURE 10 SHOWING PLASMA DAMAGE AT THE
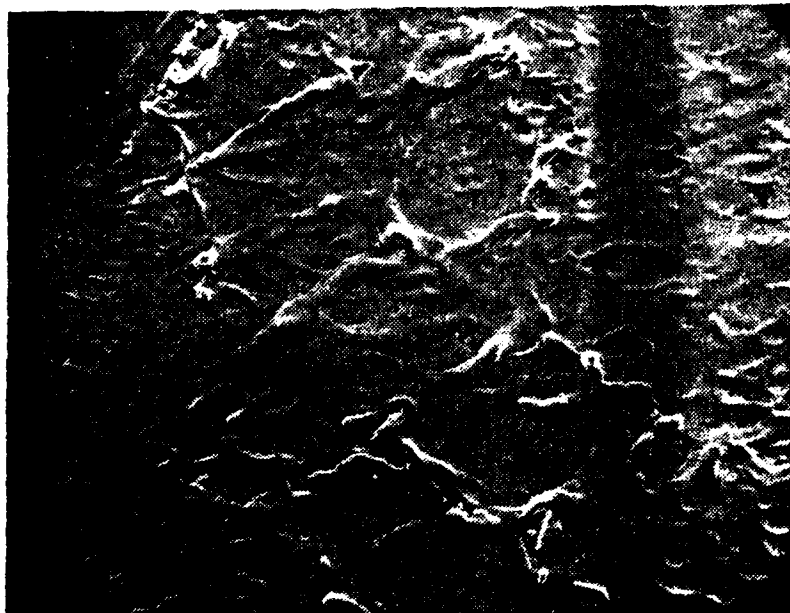PERIMETER OF THE CENTRAL CRATER. (1000X SEM)

FIGURE 12. VACUUM IRRADIATED STAINLESS STEEL. THIS VIEW SHOWS THE CENTER
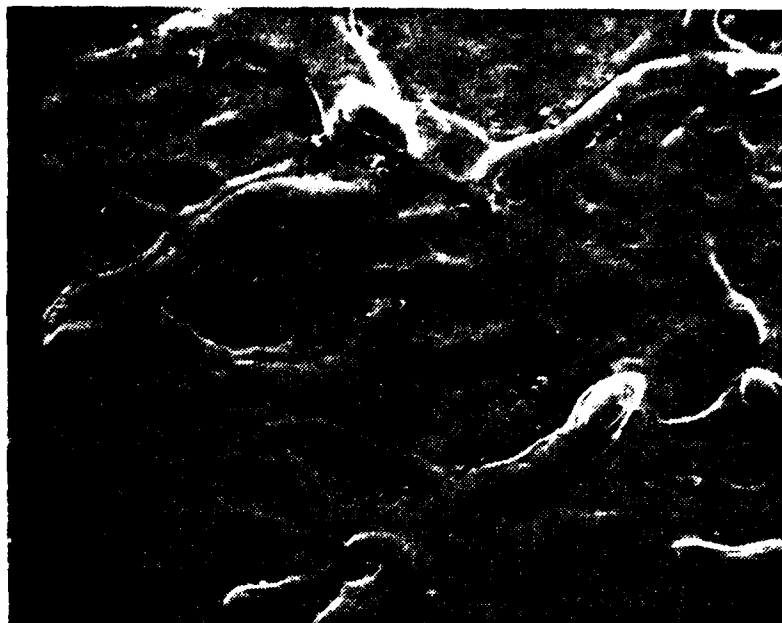OF MAIN LASER DAMAGE AREA. NOTE UNIPOLAR ARC CRATERS. (200X SEM)

39

FIGURE 13. VACUUM IRRADIATED STAINLESS STEEL. THIS IS AN ENLARGEMENT OF
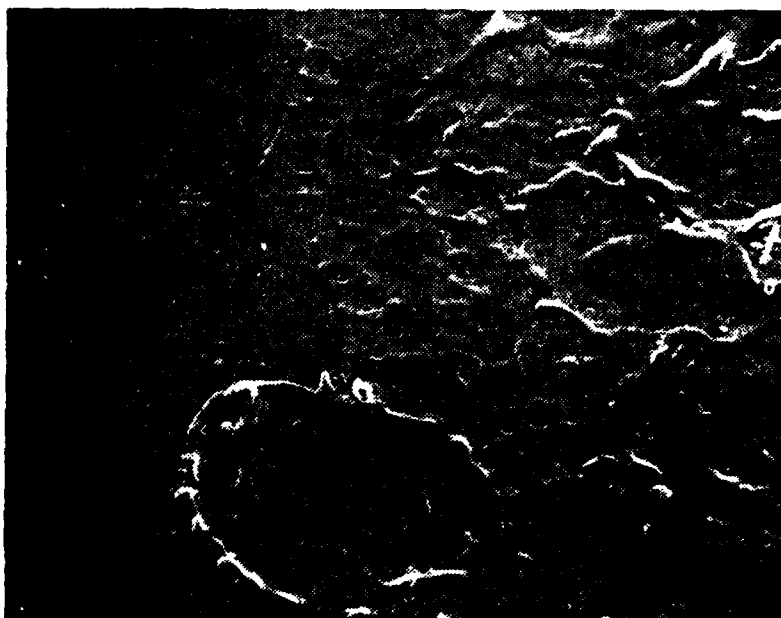THE CENTRAL CRATER SHOWING MOLTEN CENTER. (500X SEM)

FIGURE 14. VACUUM IRRADIATED STAINLESS STEEL. THIS VIEW SHOWS THE OUTER
PERIMETER OF THE CENTRAL CRATER. THE CENTRAL CRATER IS TO THE
RIGHT. NOTE THE PLASMA DAMAGE CAUSED BY UNIPOLAR ARCS AS THE
PLASMA CLOUD EXPANDED ACROSS THE STEEL. (200X SEM)

and number of these craters decreases with increasing distance from the center of damage. This photograph clearly indicates where the thermal effects of the laser-plasma interaction ended. Unipolar arcing, however, continued for some distance beyond the thermal effect limit. The diameter of the large unipolar arc crater in the left hand corner was 0.15 mm.

     b.   Uncoated Stainless Steel Irradiated in
         Air at Atmospheric Pressure

A second sample of stainless steel was irradiated in air at atmospheric pressure. This sample was prepared in the same manner as the sample that was vacuum tested. Figure 15 is an optical microscope photograph of the main crater. Hundreds of small craters are present in the primary damage area. Figure 16 was taken by the optical microscope at the perimeter of the primary crater. The center of the main crater is at the photograph's lower left corner. The elongated damage areas seen in the photograph's upper right hand corner were created by molten steel splattering over the surface of the sample and rapidly cooling.

Several small craters are located near Figure 16's upper center and upper left corner. Figure 17 is a SEM photograph of a honey-comb effect located in the primary damage area. Except for the honey-combed areas, the surface is smooth with only a few craters.

Figure 18 gives a wider field of view at 500X of the area shown in Figure 17. A few dimples and craters can be seen at the edges of the photograph. The diameter of the
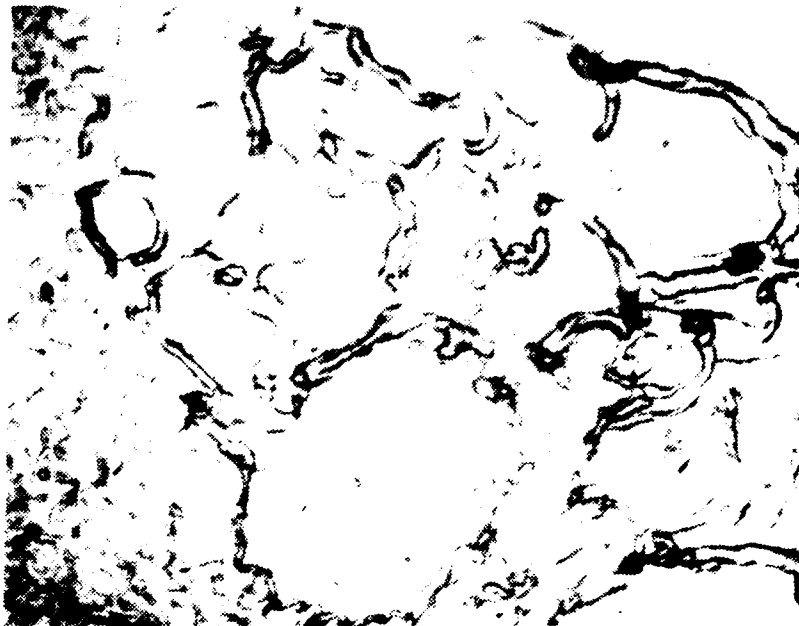
41

FIGURE 15.   STAINLESS STEEL IRRADIATED IN AIR.   THIS OPTICAL MICROSCOPE
VIEW SHOWS THE CENTRAL CRATER WITH A LARGE MOLTEN AREA, MANY
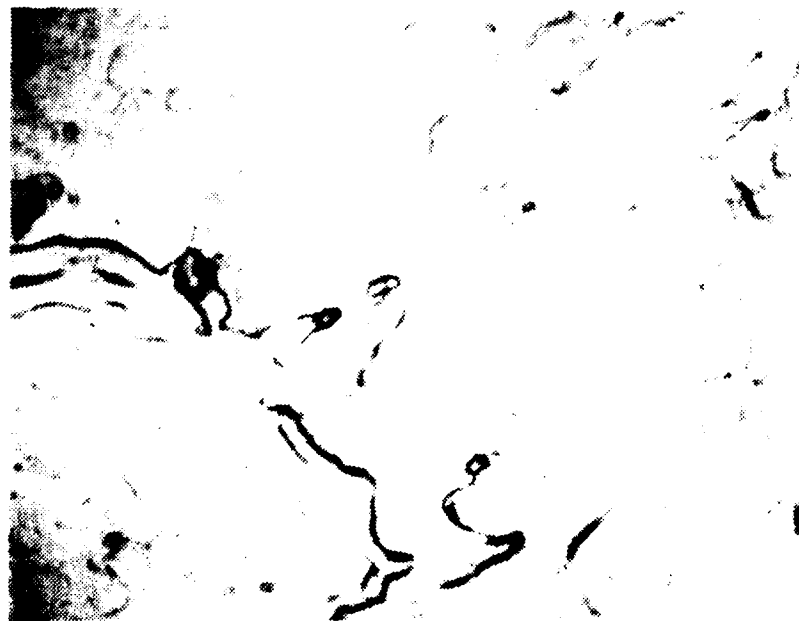SMALL CRATERS ARE PRESENT.   (100X)

FIGURE 16.   AIR IRRADIATED STAINLESS STEEL SHOWING OUTER PERIMETER OF THE
MAIN CRATER.   NOTE THE SPLATTERED STEEL.   (200X OPTICAL MICRO-
SCOPE)

42

FIGURE 17. AIR IRRADIATED STAINLESS STEEL. THIS VIEW SHOWS THE MOLTEN
AREA IN THE CENTRAL CRATER. (1000X SEM)

FIGURE 18. WIDE ANGLE VIEW OF AIR IRRADIATED STAINLESS STEEL. THE MAIN
CRATER IS TO THE RIGHT. THE ONSET OF PLASMA DAMAGE CAN BE
SEEN AT THE LEFT. (500X SEM)

43

damaged area is 2.0 mm. The main crater is 25 μm deep and is 0.88 mm in diameter. Figures 19 and 20 were taken beyond the perimeter of the laser impact area. These photographs show craters caused by unipolar arcing. The arc craters are 3 to 4 μm in diameter.

c. Stainless Steel Plasma Interaction Comments

When the stainless steel was irradiated in a vacuum, both unipolar arcing and thermal effects were present as the plasma cloud expanded from the center of the main crater radially outward. Unipolar arcing caused a cratering effect near the center of laser damaged area. These early craters were smoothed by surface melting.

As shown in Figure 14, once the plasma cloud had expanded about 1.0 mm from the center of the laser-steel interaction, surface melting ceased. Craters caused by unipolar arcing were the major damage mechnaism in the area outside the laser impact point.

The melting and boiling points of any substance are pressure dependent. Although it is very difficult to calculate the vapor pressure of a material during a laser-surface interaction, the metal vapor pressure may be substantially different at atmospheric pressure than at 10^{-6} torr.

A comparison of the damage caused by the laser when the sample was irradiated in a vacuum and at atmospheric pressure is given below:

FIGURE 19. AIR IRRADIATED STAINLESS STEEL. THIS IS A VIEW OF THE OUTER
PERIMETER OF THE MAIN CRATER AND SHOWS WHERE THERMAL EFFECTS
STOPPED. NOTE UNIPOLAR ARCING CRATERS AT THE BOTTOM OF THE
PHOTOGRAPH. (500X SEM)

FIGURE 20. AIR IRRADIATED STAINLESS STEEL. OUTER VIEW OF THE MAIN CRATER
SHOWING THE EFFECTS OF UNIPOLAR ARCING. (500X SEM)

	Vacuum	Atmospheric Pressure
Total diameter of damaged area	2.3 mm	2.0 mm
Main laser crater diameter	1.27 mm	0.88 mm
Main laser crater depth	65 μm	25 μm
Average arc crater diameter	15 μm	3.5 μm

As can be seen from the data given above, more damage was done when the sample was irradiated in a vacuum than when it was irradiated in air at atmospheric pressure.

The conclusion to be drawn is that when a laser interacts with stainless steel with sufficient energy to cause vaporization and plasma formation, a central damage crater is created at the immediate laser impact point. The depth and diameter of this central crater for equal amounts of laser power will be larger when the sample is irradiated in a vacuum than when the sample is irradiated in an atmosphere at a higher pressure. Beyond the perimeter of the laser impact point, the surface of the steel is melted as the hot plasma expands radially across the sample's face. The total area of the plasma damage is greater when the sample is irradiated in a vacuum.

The above observations can be explained by the following model. When a laser interacts with the steel surface, the depth and diameter of the crater at the laser impact point is dependent upon the laser's power, the length of the laser

46

pulse and the atmospheric pressure. If the steel sample is irradiated at atmospheric pressure, some of the laser's energy will be expended ionizing the gases just above the steel surface. Therefore, the impact crater will be smaller than if the steel was irradiated in a vacuum where there is no gas to ionize. Once vaporization of the steel followed by plasma formation has begun, the expanding plasma craters and melts the area immediately adjacent to the laser light impact point. This melting occurs only on the immediate surface of the steel. If the plasma is expanding against an atmosphere, a portion of the plasma's energy is expended ionizing the atmosphere. Therefore, less surface melting will occur at higher pressures. The area of surface melting extends for a finite radius around the laser impact point. The length of this molten radius is controlled by the rate of plasma cooling. In a vacuum, the molten radius is larger because the plasma is not being cooled by expending energy to ionize the atmospheric gas. Beyond the molten radius, the plasma cloud retains a sufficient amount of energy to cause isolated and very distinct arcing craters as it interacts with the steel surface. The radius of this cratered region is dependent upon the amount of energy remaining in the plasma and will be greater in a vacuum than at higher pressures.

2. Nickel

a. Nickel Irradiated in a Vacuum

The 0.25 mm thick sheet of nickel used in this test was prepared in accordance with Reference 12. The specimen was

47

irradiated in a vacuum with 3.5 joules of energy. The damaged area had a diameter of 1.52 mm with a depth of 45 μm. The main crater was 0.80 mm in diameter and was deep only at the center. Figure 21 is an optical microscope 100X photograph of the primary damage area. Figure 22 is a SEM view of the main crater's center. The only visible damage is the obvious molten area and a few large dimples or craters. Figure 23 was taken immediately adjacent to the main crater. This area is almost damage free. The laser impact position is at the photograph's top.

Some cratering damage can be seen in Figure 24. The main crater is at the photograph's lower right corner. However, the amount of cratering from the plasma-surface interaction is small as evidenced by Figure 25 which is a SEM photograph taken at the upper perimeter of the damaged area.

b. Nickel Irradiated in Air at Atmospheric Pressure

The specimen that was used above was cut in half. The undamaged half of the specimen was then irradiated in air at atmospheric pressure. Figures 26 and 27 are 100X photographs of the center of the damage area taken by the optical microscope and the SEM, respectively. The damaged area was 1.6 mm in diameter and 45 μm deep. Figure 27 shows thermal damage around the center of the damaged area. To the left of the damage center, evidence of melting is obvious. At a higher magnification of 200X in Figure 28, there is no evidence of cratering caused by unipolar arcing.

48

FIGURE 21. NICKEL IRRADIATED IN A VACUUM. THE LARGE CENTRAL DAMAGE AREA OF THE CRATER IS AT THE RIGHT. (100X OPTICAL MICROSCOPE)

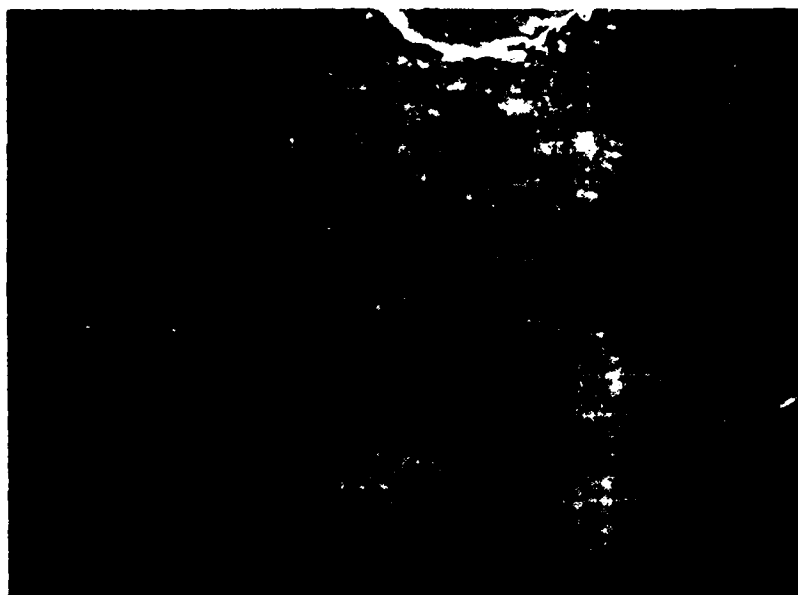FIGURE 22. NICKEL IRRADIATED IN A VACUUM. PHOTOGRAPH OF CENTER OF MOLTEN CRATER. (500X SEM)

44

FIGURE 23. NICKEL IRRADIATED IN A VACUUM. VIEW JUST BEYOND PERIMETER OF MAIN CRATER. NOTE ABSENCE OF ARC CRATERS.
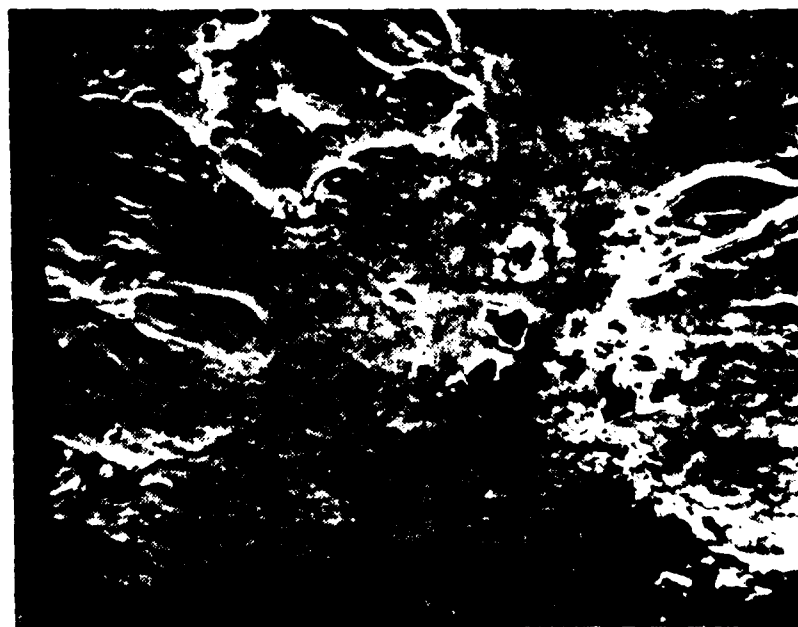

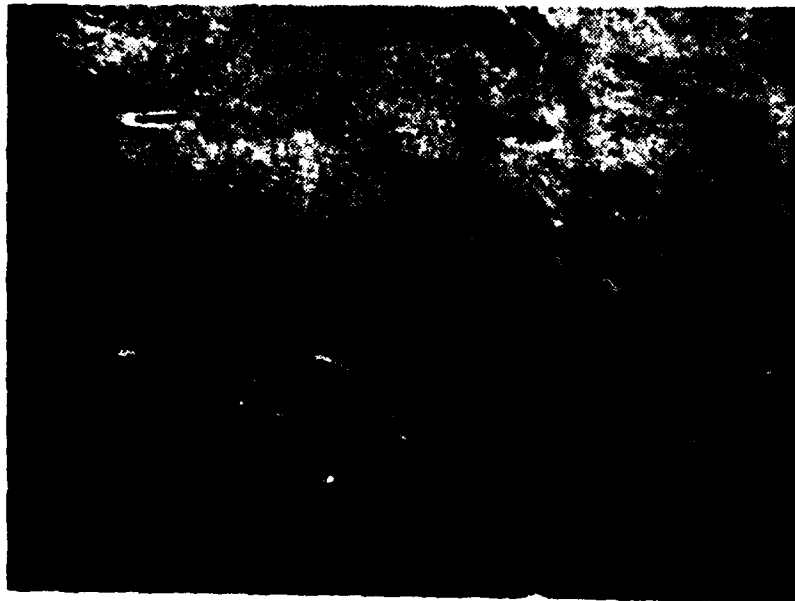FIGURE 24. NICKEL IRRADIATED IN A VACUUM. VIEW NEAR CENTER OF MAIN AREA. (200X SEM)

FIGURE 25. NICKEL IRRADIATED IN A VACUUM SHOWING OUTER PERIMETER OF MAIN
CRATER. (500X SEM)
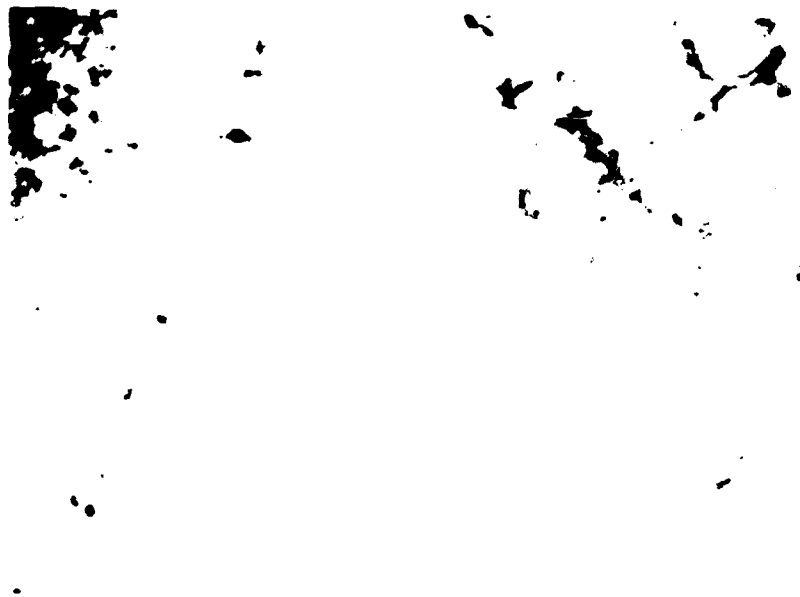
FIGURE 26. NICKEL IRRADIATED IN AIR SHOWING PRIMARY MOLTEN CRATER.
(500X OPTICAL MICROSCOPE)

FIGURE 27. NICKEL IRRADIATED IN AIR SHOWING PRIMARY DAMAGE AREA.
(100X SEM)
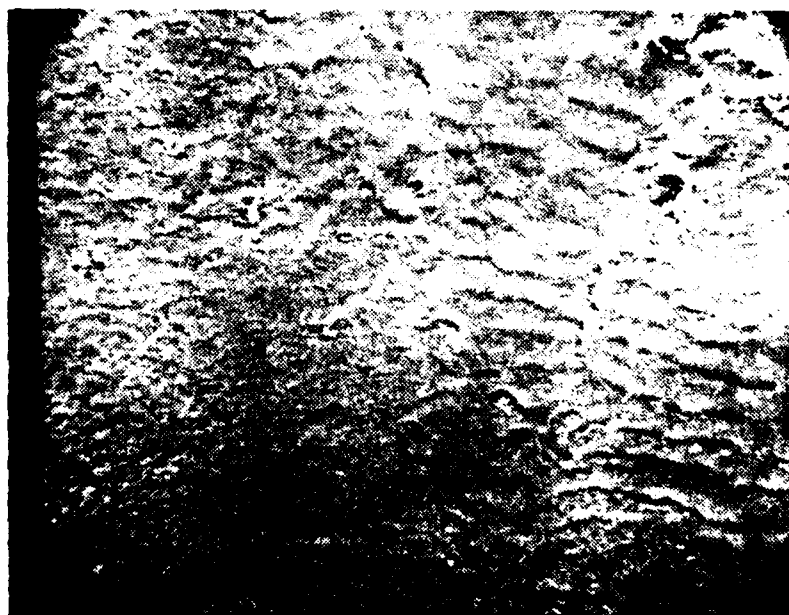
FIGURE 28. NICKEL IRRADIATED IN AIR SHOWING OUTER PERIMETER OF THE MAIN
DAMAGE AREA.   (200X SEM)

c. Nickel Plasma Interaction Comments

When the nickel was irradiated in a vacuum, the nickel laser interaction was characterized by a large molten metal primary damage area. Beyond the perimeter of the central damage agea, the sample was almost damage free.

Craters, which would indicate the presence of unipolar arcing, are almost entirely absent. The few craters that were present were small in comparison with the craters on the stainless steel sample. The absence of recognizable cratering beyond the primary damage area, indicates that the expanding plasma did not strongly interact with the nickel surface.

A comparison of the damage caused by the laser when the sample was irradiated in air and at atmospheric pressure is given below:

	Vacuum	Atmospheric Pressure
Total damage area diameter	1.52 mm	1.60 mm
Main crater diameter	0.80 mm	0.80 mm
Depth of main crater	45 μm	45 μm

As can be seen from the above data, there is a negligible difference between the two samples. This is an unexpected finding that is in contrast to the observations made with stainless steel. This result may indicate that nickel is more resistant to laser-plasma damage mechanisms.

A surprising aspect of the nickel sample was the almost complete absence of unipolar arcing craters. Figures 27 and 28 indicate that a hot plasma was formed outside the central damage area melting the surface there. There were only a few craters visible in this area, however. This suggests that nickel may be resistant to unipolar arcing damage.

3. Copper

a. Copper Irradiated in a Vacuum

A 0.375 mm thick sample of copper was prepared and irradiated in the test chamber at a vacuum of 10^{-6} torr. The power of the laser beam was 3 joules resulting in a damaged area 2 mm in diameter. Figures 29 and 30 show the outer perimeter of the damaged area. The dark areas scattered outside of the major damaged area were probably caused by a plasma-surface interaction.

The center of the 25 μm deep main crater is shown in Figure 31. The layered rosette pattern indicates that the copper sample was in a highly molten state for a relatively long time. Figures 32 to 34 show the many dimpled craters formed aroung the outer perimeter of the damaged area. The larger craters were formed first while the younger craters appear as small dimples. The many new craters, seen at the top of Figure 33, average .002 mm in diameter. The larger craters are .015 mm in diameter and 2 to 4 μm deep.

54

FIGURE 29. COPPER IRRADIATED IN A VACUUM SHOWING THE OUTER PERIMETER OF
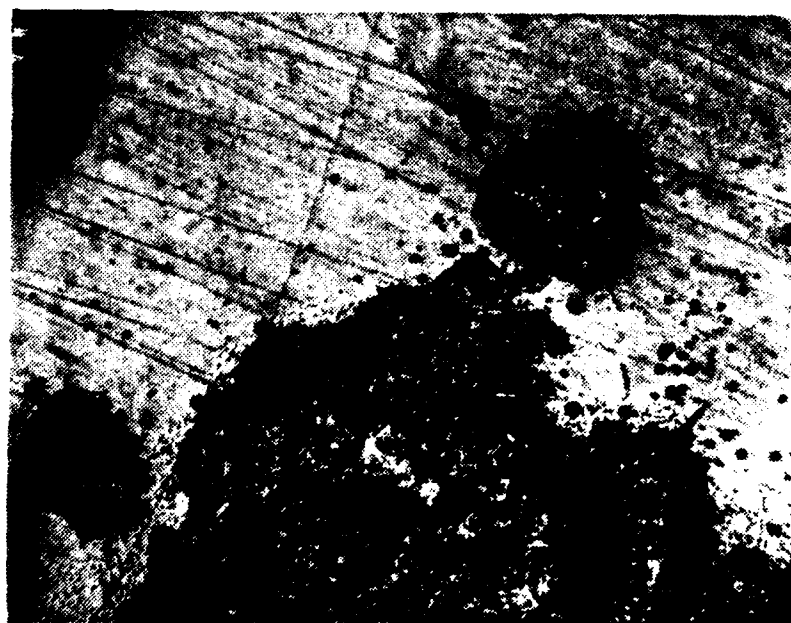THE MAIN CRATER. (200X OPTICAL MICROSCOPE)

FIGURE 30. COPPER IRRADIATED IN A VACUUM SHOWING DAMAGE AT PERIMETER OF
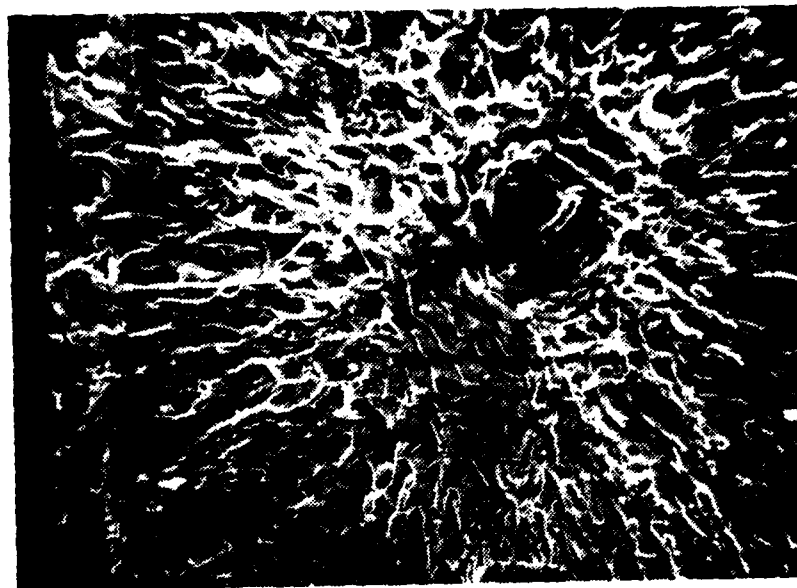THE MAIN CRATER. (200X OPTICAL MICROSCOPE)

FIGURE 31.   COPPER IRRADIATED IN A VACUUM.   CENTER OF LASER IMPACT AREA.
(500X SEM)

FIGURE 32.   COPPER IRRADIATED IN A VACUUM.   PERIMETER OF PRIMARY DAMAGE
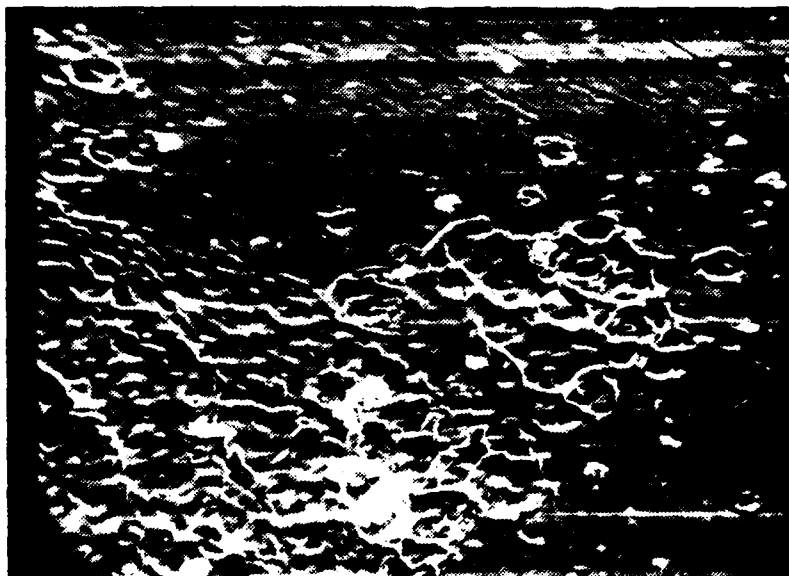AREA SHOWING UNIPOLAR ARCING CRATERS.   (500X SEM)

FIGURE 33. COPPER IRRADIATED IN A VACUUM SHOWING OUTER PERIMETER OF THE
MOLTEN DAMAGE AREA.   (500X SEM)

FIGURE 34. COPPER IRRADIATED IN A VACUUM.   VIEW OF UNIPOLAR ARCING CRATERS.
(1000X SEM)

b.   Copper Irradiated in Air at Atmospheric Pressure

A sample of copper was irradiated in air at atmospheric pressure. The center of the main crater, Figure 35, is 20 μm deep. The overall damaged area is 2 mm in diameter.

Figure 36 is a SEM photograph of the central crater. The primary damage area at the focal point of the laser is highly molten. Metal is splattered to the outer perimeter of the crater as shown in Figure 36. Unipolar arcing craters can be seen just beyond the perimeter of the main crater in this photograph. These unipolar arcing craters are enlarged in Figures 37 and 38.

c.   Copper Plasma Interaction Comments

The photographs clearly show that copper is highly susceptible to damage from unipolar arcing. Cratering caused by unipolar arcing is readily apparent at the outer perimeter of the primary damage area.

Comparing Figures 31 and 36 show that the copper experienced a much more violent reaction to the laser pulse when it was irradiated in a vacuum that at atmospheric pressure. The size and density of the unipolar arcing craters is much greater in the vacuum than at atmospheric pressure. In Figure 33 (vacuum) the unipolar craters are 12.5 μm in diameter and their density is about 2000 per cm^2. In Figures 37 and 38 (atmospheric pressure) the unipolar craters are 8-10 μm in diameter and their density is still about 2000 cm^2.
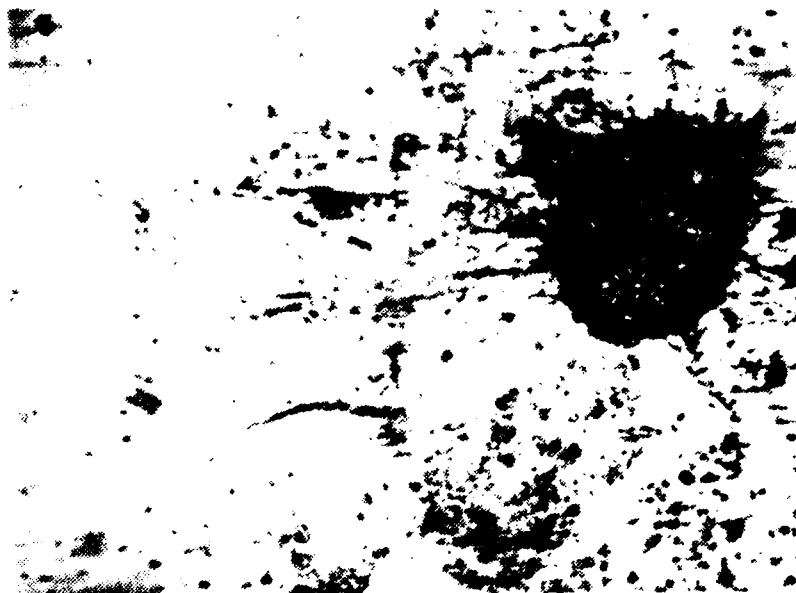
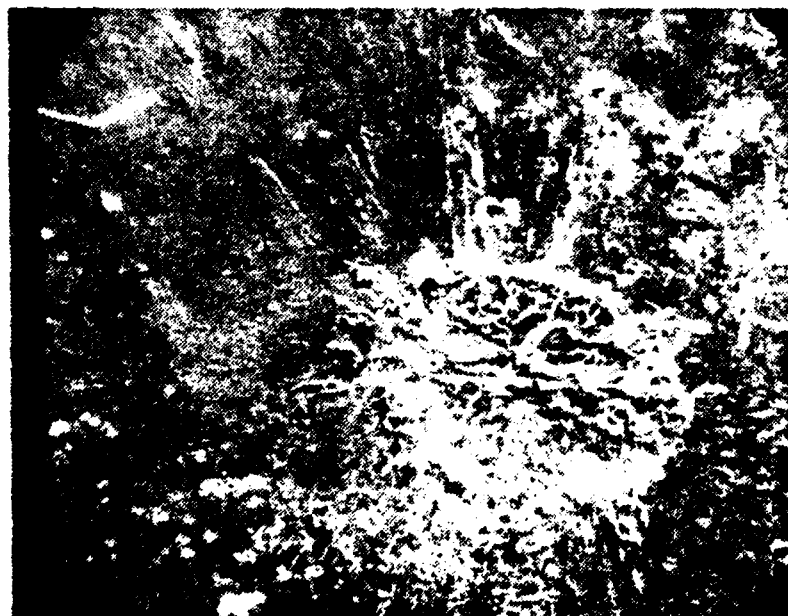FIGURE 35. COPPER IRRADIATED IN AIR. PRIMARY DAMAGE AREA. (100X OPTICAL MICROSCOPE)

FIGURE 36. COPPER IRRADIATED IN AIR. PRIMARY DAMAGE AREA. (200X SEM)
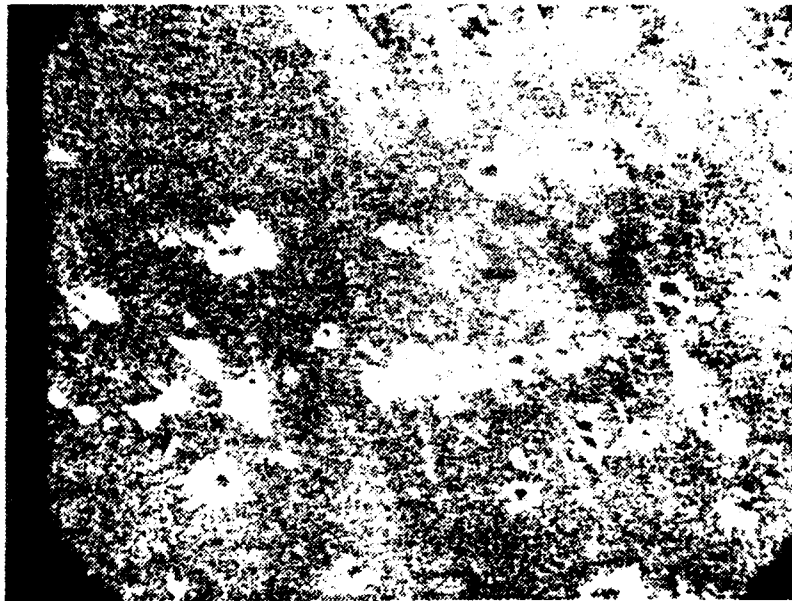
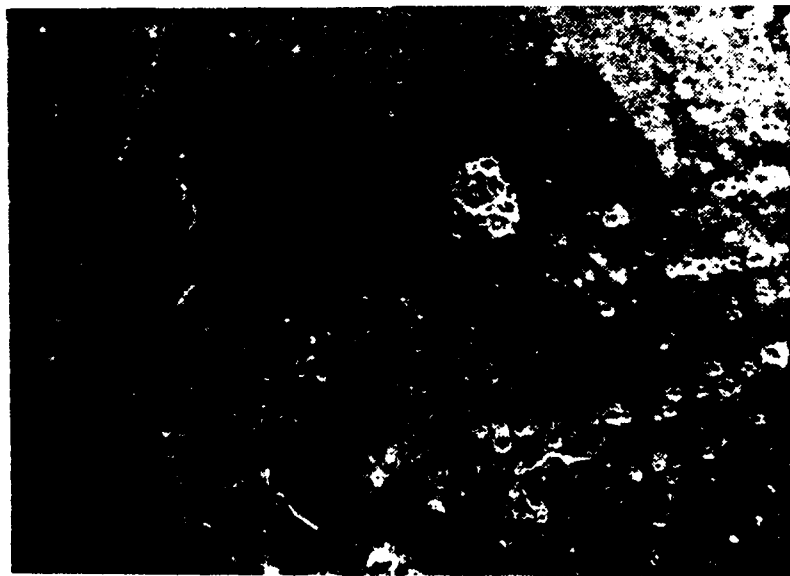FIGURE 37.   COPPER IRRADIATED IN AIR SHOWING UNIPOLAR ARCING CRATERS.
(500X SEM)

FIGURE 38.   COPPER IRRADIATED IN AIR SHOWING MULTIPLE UNIPOLAR ARC CRATERS.
(200X SEM)

4. **Tin**

a. Tin Irradiated in a Vacuum

A sample of tin 0.375 mm thick was irradiated with 2.83 joules of energy in the test chamber at 10^{-6} torr vacuum. Figure 39 is an optical microscope photograph of the damage caused by the laser-tin interaction. Molten metal is splattered about the perimeter of the main damaged area. The SEM photograph, Figure 40, is another view of the 35 μm deep main crater. The gash at the left of the photograph is part of a line scribbed into the metal after the test to help locate the damaged areas for the SEM.

Figures 40 and 41 are a series of views of the upper perimeter of the damaged area. Figure 41 shows what appears to be an abrupt end of the damaged area. At a higher magnification (Figures 42 and 43), small arcing craters beyond the outer perimeter of the molten damage are evident.

Another tin sample was irradiated. The second main crater, Figures 44 and 45, looked essentially the same as the first main crater (Figure 40). Figures 46 to 49 show a large molten area.

Figure 46 was taken at the main crater's outer perimeter. The large crater in the center of the photograph appears to be an area of concentrated plasma damage. Figure 47, a view of the opposite side of the primary crater from Figure 46, shows a similar damage mechanism. A higher magnification of these areas, Figures 48 and 49, verify that the large molten spots are actually a concentration of many craters resulting from the plasma-surface interaction.
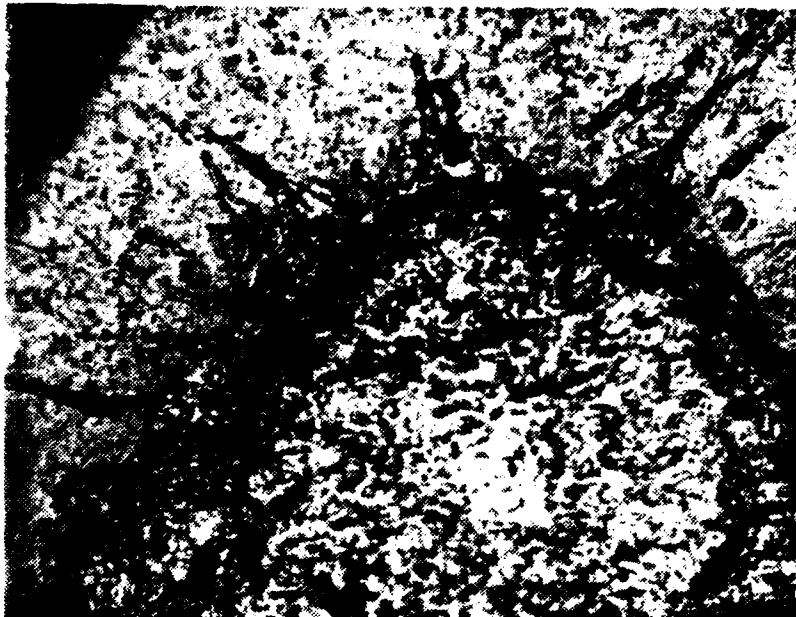
61

FIGURE 39.   TIN IRRADIATED IN A VACUUM SHOWING PRIMARY DAMAGE AREA. (200X OPTICAL MICROSCOPE)
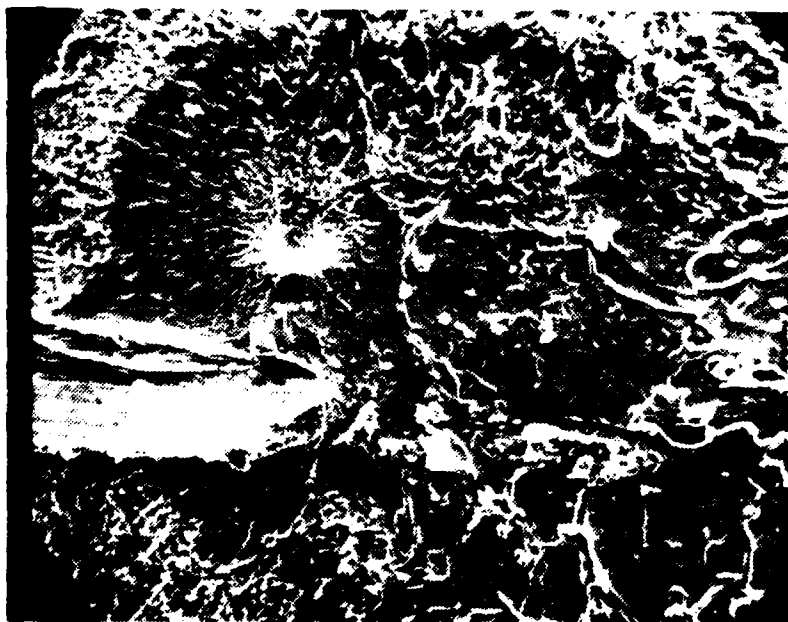

FIGURE 40.   TIN SHOWING LASER PRIMARY DAMAGE AREA.   SCRATCH AT LEFT WAS MADE AFTER LASER INTERACTION.   (100X SEM)
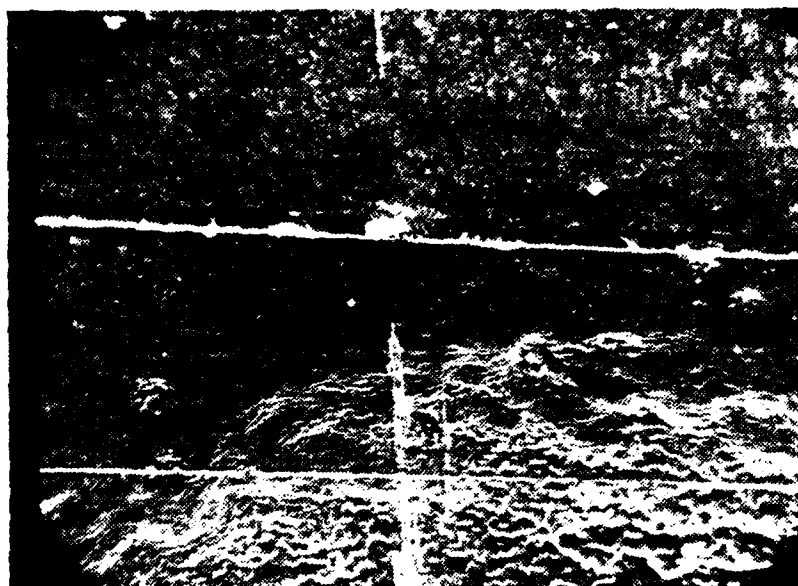
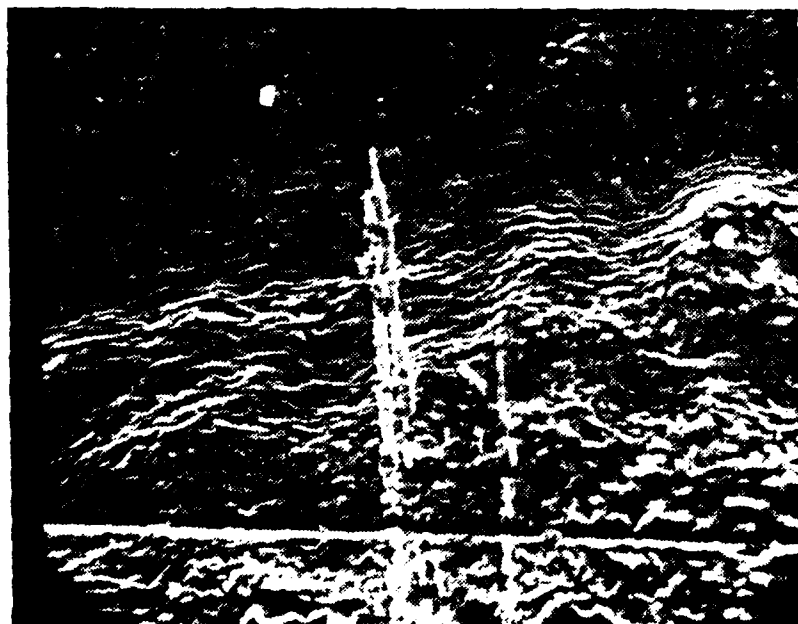FIGURE 41. TIN. OUTER PERIMETER OF MAIN DAMAGE AREA. (200X SEM)

FIGURE 42. TIN. OUTER PERIMETER OF MAIN DAMAGE AREA. (500X SEM)

FIGURE 43. TIN. OUTER PERIMETER OF MAIN DAMAGE AREA. (500X SEM)

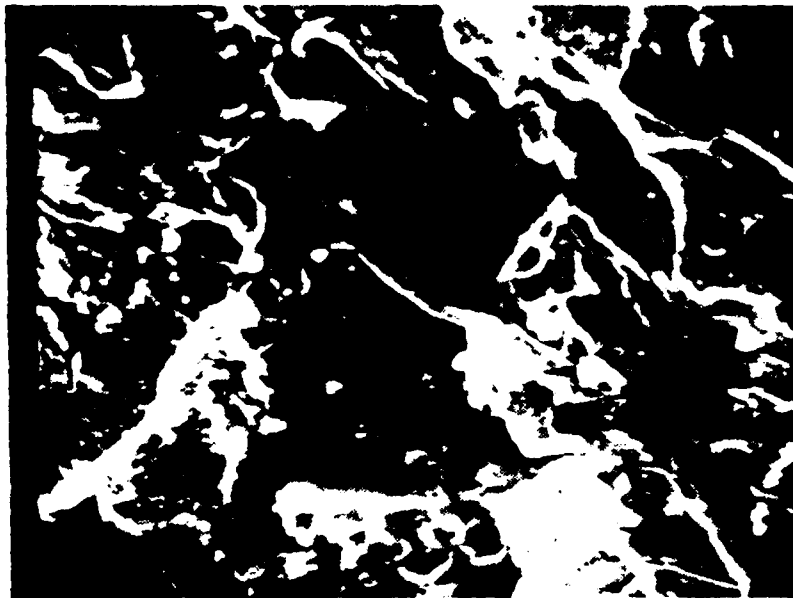FIGURE 44. TIN. CENTER OF PRIMARY DAMAGE AREA. (200X SEM)

FIGURE 45. TIN. PRIMARY LASER DAMAGE AREA. (500X SEM)

FIGURE 46. TIN. OUTER PERIMETER OF LASER DAMAGE AREA. (200X SEM)

68

FIGURE 47.   TIN.   OUTER PERIMETER OF PRIMARY LASER DAMAGE AREA. (500X SEM)
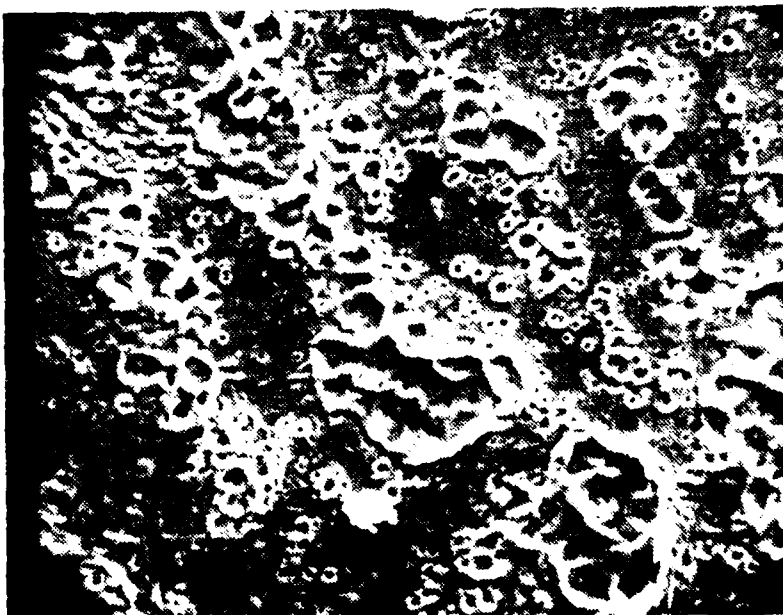

FIGURE 48.   TIN.   OUTER PERIMETER OF MAIN DAMAGE AREA.   (500X SEM)
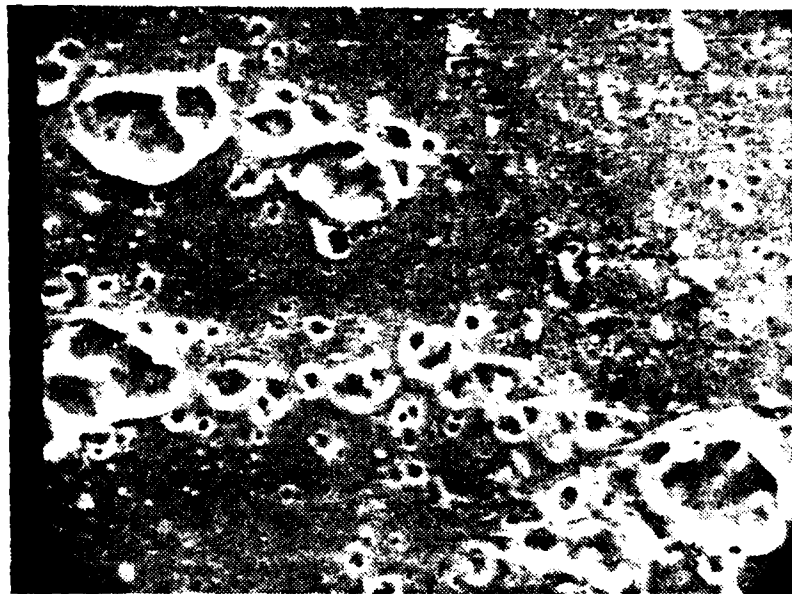
FIGURE 49. TIN. MAGNIFIED VIEW OF UNIPOLAR ARCING CRATERS. (1000X SEM)

b.   Tin Plasma Interaction Comments

The tin sample showed a typical laser-light inter-action which led to plasma formation and plasma-surface interaction. The central craters, Figures 40 and 44, were characterized by a high degree of thermal interaction which resulted in a highly molten surface. Metal was splattered at the outer edges of the crater (Figure 40).

At the outer edges of the central crater, waves of molten metal can be seen (Figure 41). These waves were probably formed as a hot dense plasma expanded outward across the tin's surface. Cratering caused by unipolar arcing (Figures 42, 48 and 49) continued to occur beyond the limit of sufrace melting. The great extent of this damage shows that tin is highly sus-ceptible to plasma-surface interactions.

5. Titanium Foil

a.   Titanium Foil Irradiated in a Vacuum

A 0.025 mm thick sheet of titanium foil was irradi-ated with 3 joules. This was enough energy to burn a hole through the titanium foil.

The edges of the hole in the titanium foil were examined with the SEM. Figure 50 shows the edge of the hole at the lower left corner of the photograph. Waves of molten metal, shown in Figure 51, can be clearly seen flowing away from the central hole. Figure 52 is an enlarged view of the outer molten area. A few craters that are characteristic of unipolar arcing can be seen near the center of Figure 52.

68

These craters are about 6 μm in diameter and have smooth edges indicating that the surface was still molten after the craters were formed. Figure 53 shows small unipolar arcing craters at the outer perimeter of the central damage area indicating that plasma-surface interactions extended for some distance beyond the area of the laser impact damage.

b. Titanium Foil Interaction Comments

The laser burned through the titanium foil sample. Therefore most of the laser's energy was not employed supplying energy to the titanium sheet. As could be expected, less plasma would be formed in this case than with the previous samples which absorbed the entire energy of the laser pulse.

In spite of this, a large molten area is present around the perimeter of the laser hole. This molten area extended from the edge of the hole for 0.3 mm. Inside the molten area craters (shown in Figure 52) are evidence of arcing. This suggests that titanium is very susceptible to unipolar arcing damage.

6. Tungsten Carbide Coated with Titanium

A 5.325 mm thick sheet of titanium coated tungsten carbide was studied with the SEM. The tungsten carbide sample had been exposed to a plasma in a Microtor tokamak at UCLA.

Evidence of arcing across the surface of the sample is seen in Figure 54. This photograph, which was taken with the optical microscope, shows distinct branched tracks that measure from 0.10 to 0.15 mm across. Figures 55 to 57 were
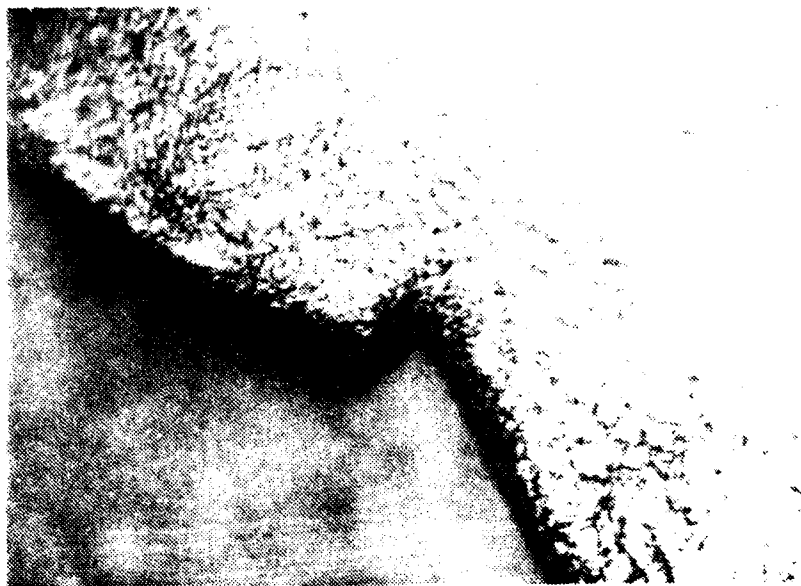
69

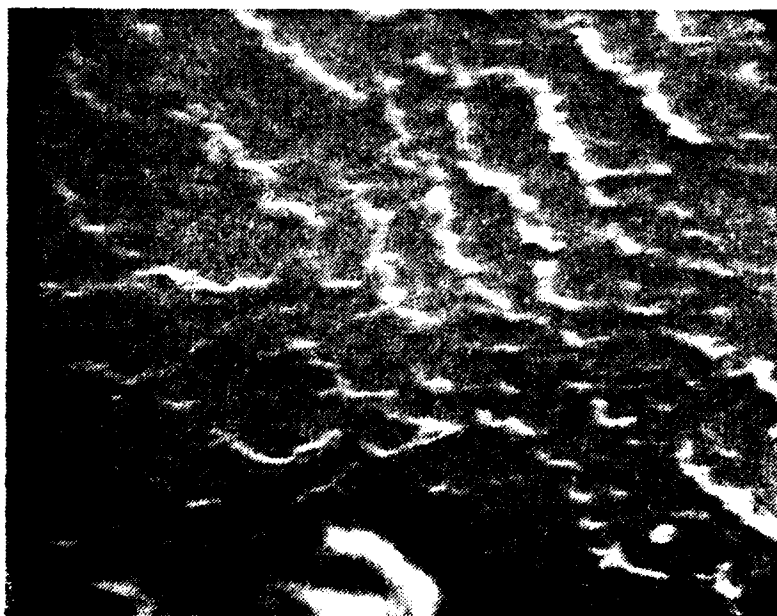FIGURE 50. TITANIUM FOIL. HOLE BURNED BY LASER IS TO THE LEFT. (100X OPTICAL MICROSCOPE)

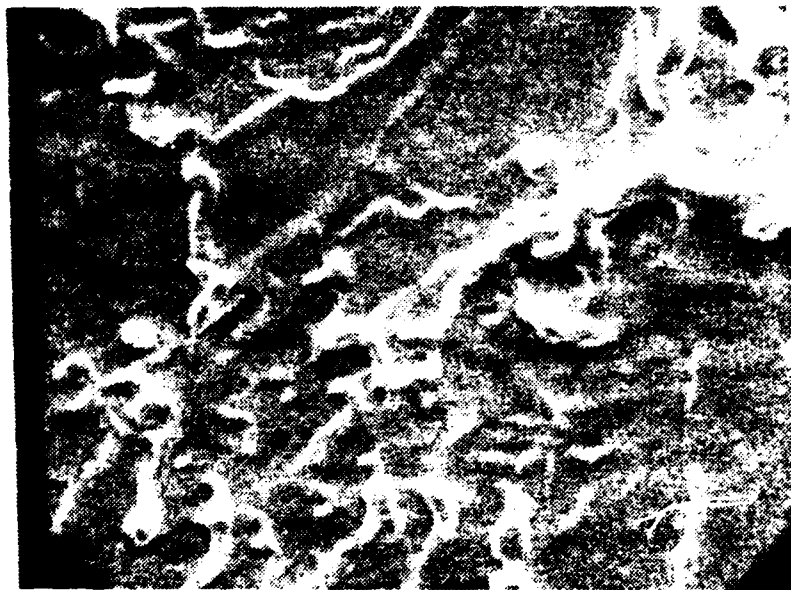FIGURE 51. TITANIUM FOIL. HOLE CAUSED BY LASER IS AT LOWER LEFT. (500X SEM)

FIGURE 52. TITANIUM FOIL. OUTER PERIMETER OF THE DAMAGED AREA. (500X SEM)
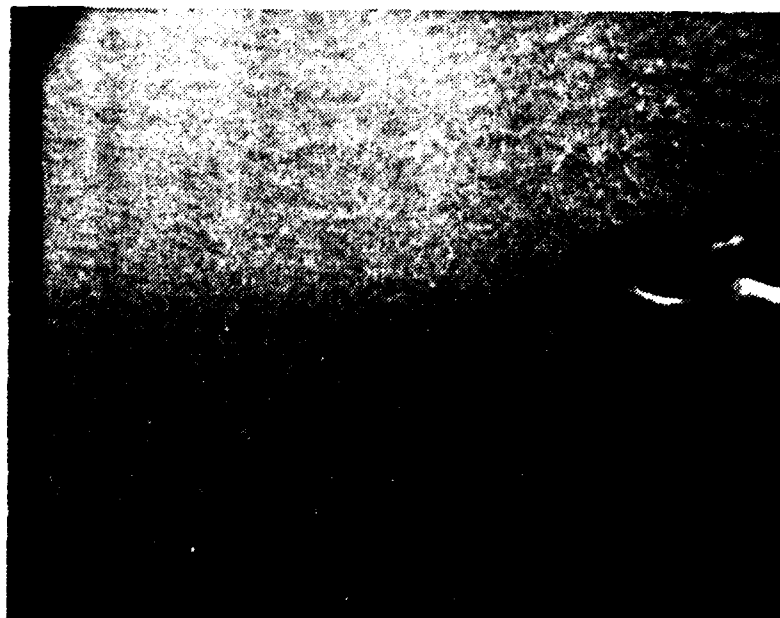

FIGURE 53. TITANIUM FOIL. LASER HOLE IS TO THE RIGHT. (200X SEM)
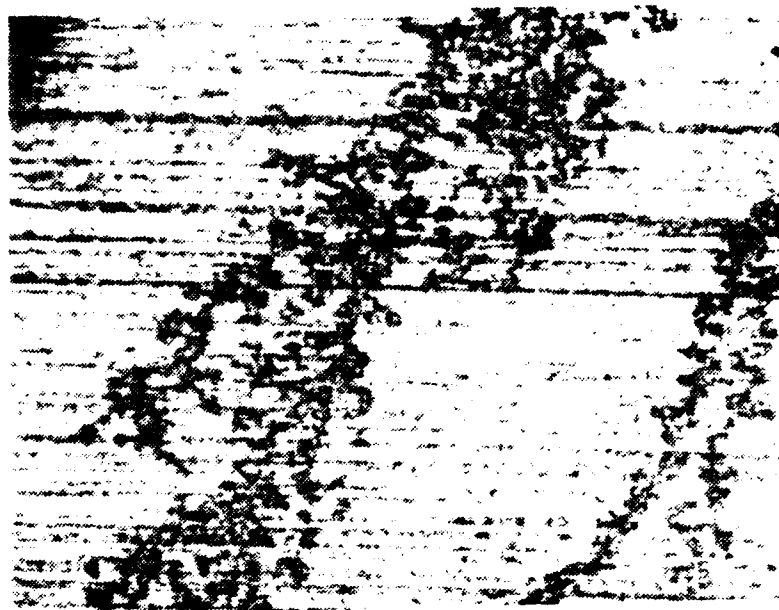
FIGURE 54.   TUNGSTEN CARBIDE COATED WITH TITANIUM ARC TRACKS INDICATES
WHERE THE Ti HAS BEEN ERODED FROM THE SURFACE.   (200X OPTICAL
MICROSCOPE)

FIGURE 55.   TUNGSTEN CARBIDE COATED WITH TITANIUM SHOWING ARC TRACKS.
(100X SEM)

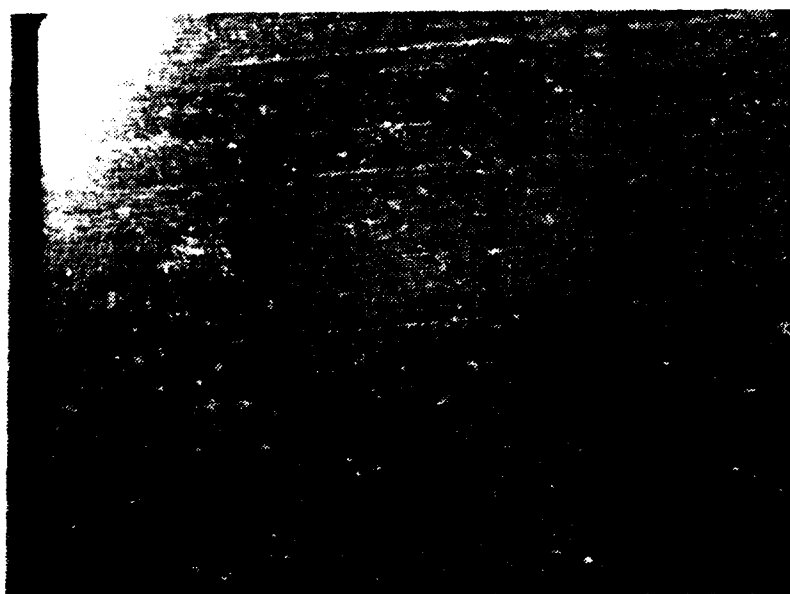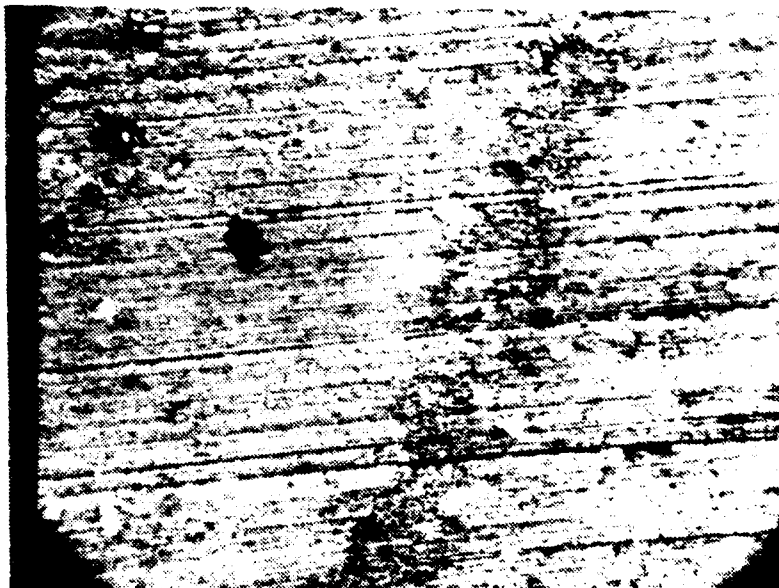FIGURE 56. TUNGSTEN CARBIDE COATED WITH TITANIUM. INDIVIDUAL CRATERS
ARE VISIBLE WHERE Ti HAS BEEN ERODED FROM THE SURFACE.
(200X SEM)

FIGURE 57. TUNGSTEN CARBIDE COATED WITH TITANIUM SHOWING CRATERING THAT
ERODED Ti FROM THE SURFACE. (500X SEM)

taken with the SEM. A single track measuring 0.10 mm in width can be seen running across the center of the photograph. The black spots at the left side of the photograph are pieces of debris. Figures 56 and 57 are magnified views of the track shown in Figure 55. Close observation of these two photographs show that the arc track was formed when a large number of craters were linked together. All of the tracks run in the same general direction, probably following the expansion or flow of the plasma. The arc craters forming this track averaged about 2 μm in diameter. A few craters are as large as 10 μm in diameter.

a. Plasma-Surface Interation Comments

The plasma caused extensive damage to the titanium coating on the tungsten carbide. The major damage mechanism was unipolar arcing. The arc craters were linked together to form a large arc track across the coating. It could not be determined if the arcing craters damaged the tungsten carbide underneath the coating.

7. Titanium Coated Stainless Steel

A 0.125 mm sheet of stainless steel coated with titanium was studied with the SEM. Figure 58 is a view of the titanium coated steel. In this figure the light area is titanium coating and the dark tracks are areas of stainless steel where the titanium has been removed from the sample's surface. A close inspection of Figure 58 reveals that a plasma-surface interaction removed a large percentage (estimated at 60 percent) of the titanium coating from the sample. Once the titanium coating

74

had been removed from the steel surface, extensive damage caused by evaporation and unipolar arcing took place. This created tracks across the steel surface. The average width of the tracks was 0.075 mm.

Figure 59 is a magnified view of one of the tracks. Extensive cratering can be clearly seen. This area consists of multiple craters layered upon each other. Figure 60 is an enlarged view of one large crater. This large crater in the stainless steel surface is 40 um in diameter. A large number of smaller craters surround the large one.

a. Titanium Coated Stainless Steel Comments

The titanium coated stainless steel reacted with the plasma by arcing. This caused arc tracks to extend across about sixty percent of the sample's surface. The titanium evaporated from the surface and the underlying stainless steel was heavily cratered. An interesting observation is that, like the titanium coated tungsten carbide, the arcs here tended to form distinct tracks. This pattern was not found on any of the conductors that were irradiated by a laser to induce a plasma. Both the titanium coated stainless steel and the titanium coated tungsten carbide were placed in a plasma environment, but were not irradiated by a laser.

B. NONCONDUCTORS

1. Sample Number One

This sample was one-half of a titanium coated glass tube. The tube had been exposed to a plasma in a chamber of

75

FIGURE 58.   STAINLESS STEEL COATED WITH TITANIUM SHOWING CRATERING THAT
             ERODED Ti FROM THE SURFACE.   (200X SEM)
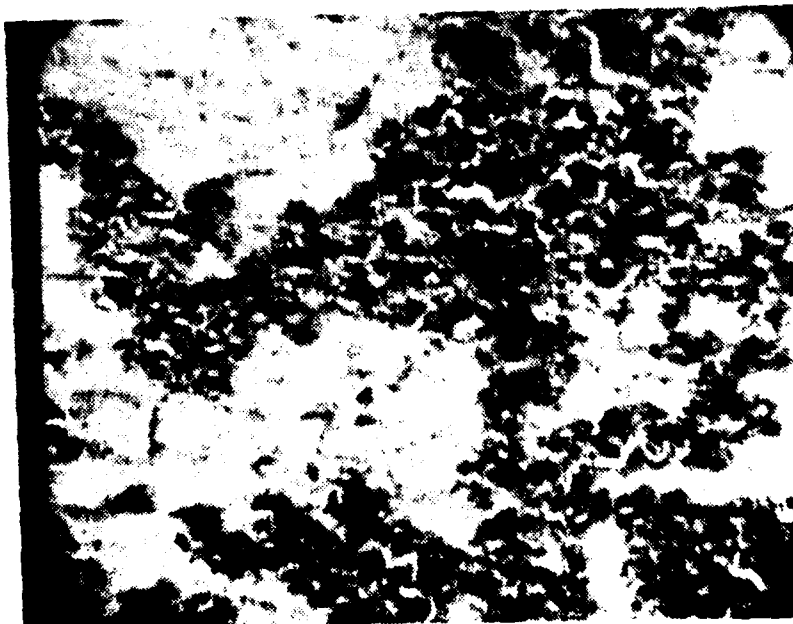

FIGURE 59.   STAINLESS STEEL COATED WITH TITANIUM.   A SERIES OF ARCS HAVE
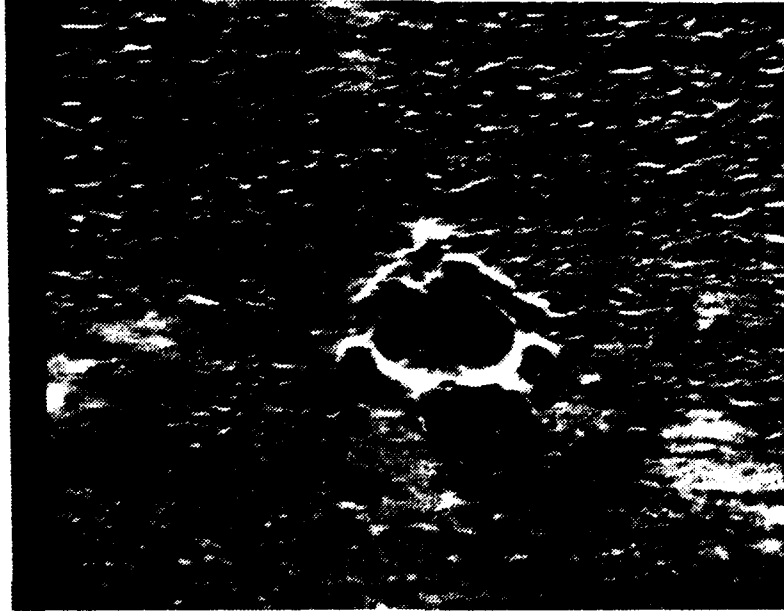   ERODED Ti FROM THE STEEL SURFACE.   (500X SEM)

FIGURE 60. STAINLESS STEEL COATED WITH TITANIUM. ENLARGED VIEW OF A
CRATER THAT ERODED THE Ti COATING. (500X SEM)

the macrotor tokamak at UCLA. Figure 5 is a photograph of this antenna shield, a tube which was 4 centimeters in diamerter and 29 centimeters long.

Figure 5 shows the extent of the arcing across the tube's surface. The black area shown in the photograph is the titanium coating. The white tracks are areas where arcing has burned away the titanium, exposing the underlying glass.

Figure 61 and 62 are enlarged views of the tube's surface. Along the lower edge of each of these figures a portion of the arc tracks have been covered with titanium that was redeposited from a Ti ball upon the glass surface after the initial arc tracks were made.

Two basic types of arcing tracks can be seen on this sample. The distinct branched tracks seen in Figure 61 appear very different from the smaller random track pattern shown in Figure 62. Figure 63 is an enlarged view of the tracks seen in Figure 61. The undamaged titanium coatings appear as grey areas while the arcing tracks are black. The arcing tracks average 0.07 mm in width. Figures 64 and 65 are enlarged views of one of the tracks. These tracks are formed by a large number of craters which have destroyed the titanium coating. Figure 65 shows a roughened surface where the titanium has been eroded from the glass. From these photographs, it is difficult to determine if the glass substrate has been damaged. The roughened surface could have been caused either by damage
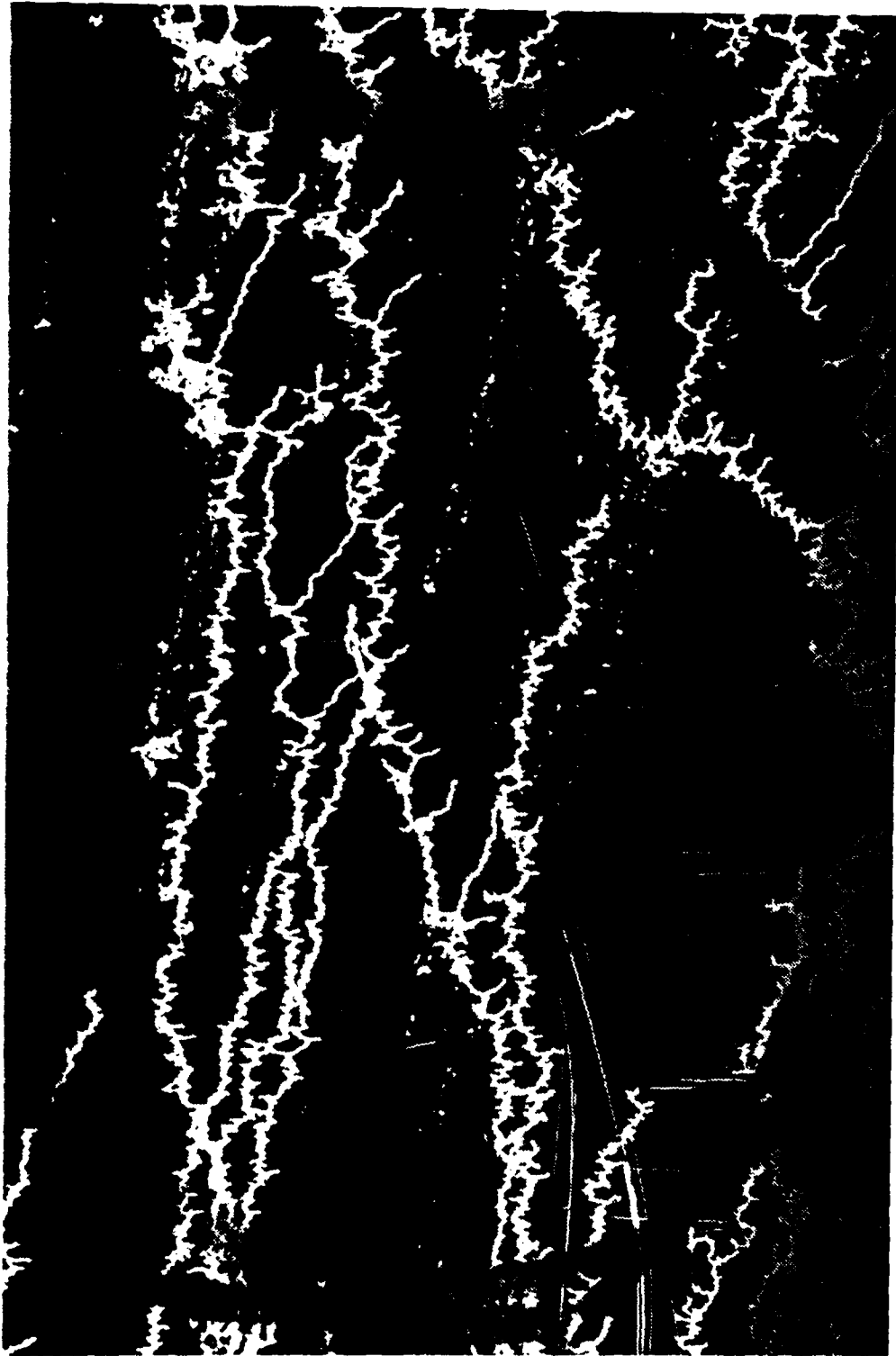
FIGURE 61. ENLARGED VIEW OF TITANIUM COATED GLASS SURFACE SHOWING ARC TRACKS.

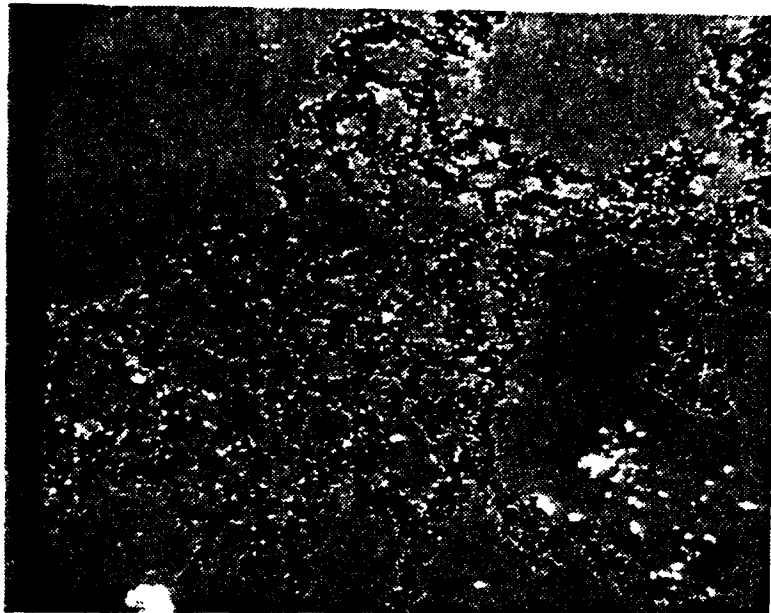FIGURE 6.2. ENLARGED VIEW OF GLASS SURFACE SHOWING FINE ARC TRACKS.

FIGURE 63. GLASS COATED WITH Ti. DISTINCT BRANCHED ARC TRASK ACROSS THE Ti COATING. (50X SEM)
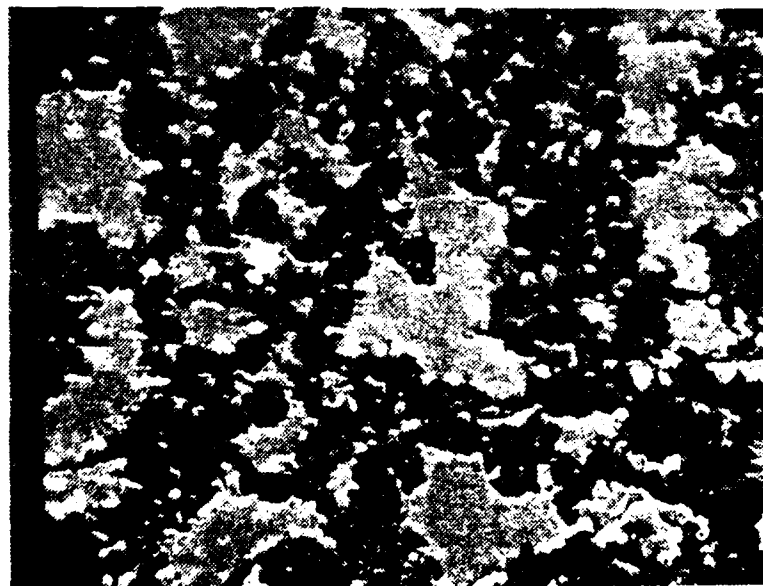

FIGURE 64. GLASS COATED WITH Ti. ENLARGED VIEW OF DISTINCT ARCING TRACKS. (200X SEM)

to the glass substrate or uneven erosion of the titanium coating. It is probable that both damage mechanisms are present.

Figures 66 to 69 are enlarged views of the random tracks shown in Figure 62. These photographs show that this region consists of randomly scattered tracks plus distinct tracks similar to the tracks shown in Figure 61. These small tracks, Figure 66, have an average width of 0.02 mm.

There are random arcing spots throughout the titanium coating. Figure 67 shows an area where there is no distinct branching pattern. The numerous damaged areas are unlinked. It is plausible that a prolonged plasma-surface interaction would cause unlinked damaged areas to develop into the larger branches seen in Figure 62. Figures 68 and 69 show that these unlinked damage areas consist of a series of linked craters.

a. Plasma-Surface Interaction Comments

This sample was damaged when arcs were established between the tube surface and the plasma. These arcs evaporated the titanium, causing craters in the titanium coating. Each new crater then seems to provide the conditions for forming a cathode-anode spot for the adjacent crater, causing a series of craters to be linked into a long, highly branched arc track. Therefore, once the arcing process started, it was progressive and ultimately resulted in an extremely damaged coating. It could not be determined if the glass surface was damaged.

82

FIGURE 65. GLASS COATED WITH TITANIUM. HIGHLY MAGNIFIED VIEW OF AN ARC TRACK. (1000X SEM)
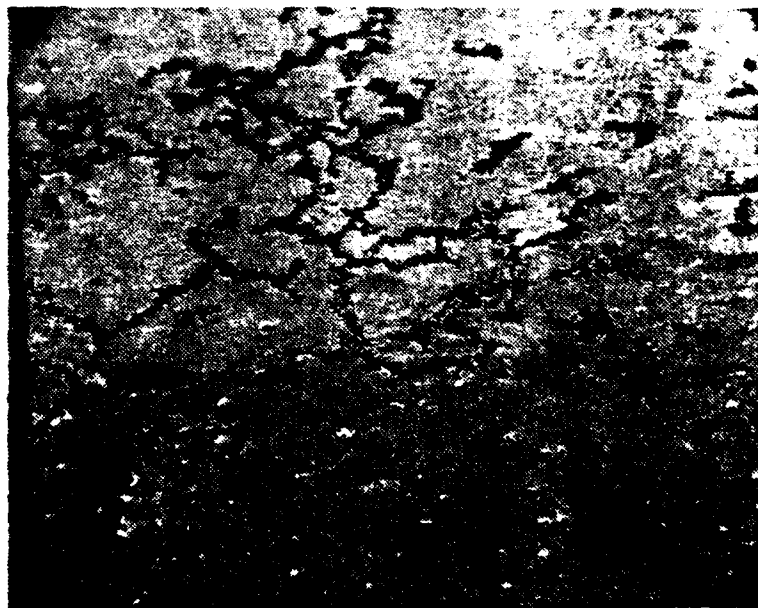

FIGURE 66. GLASS COATED WITH TITANIUM. VIEW OF THE SMALLER ARC TRACKS. (50X SEM)
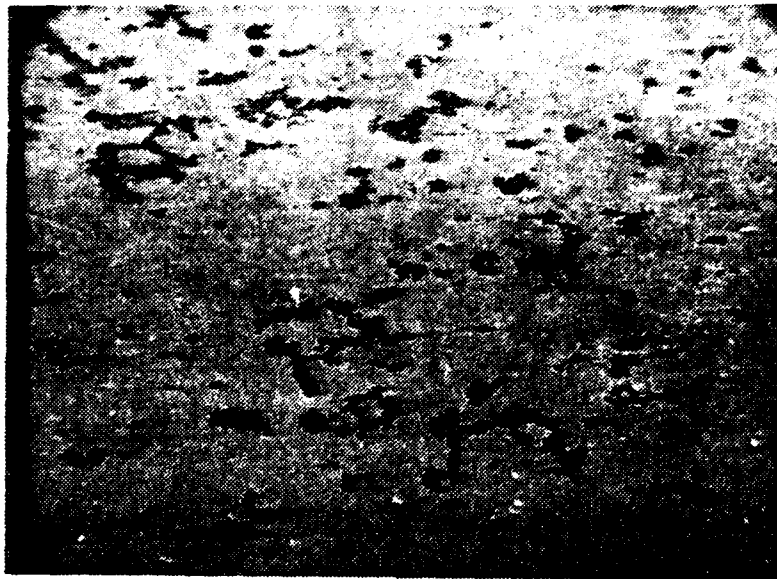
33

FIGURE 67.   GLASS COATED WITH TITANIUM SHOWING SMALLER ARC TRACKS.   (50X SEM)
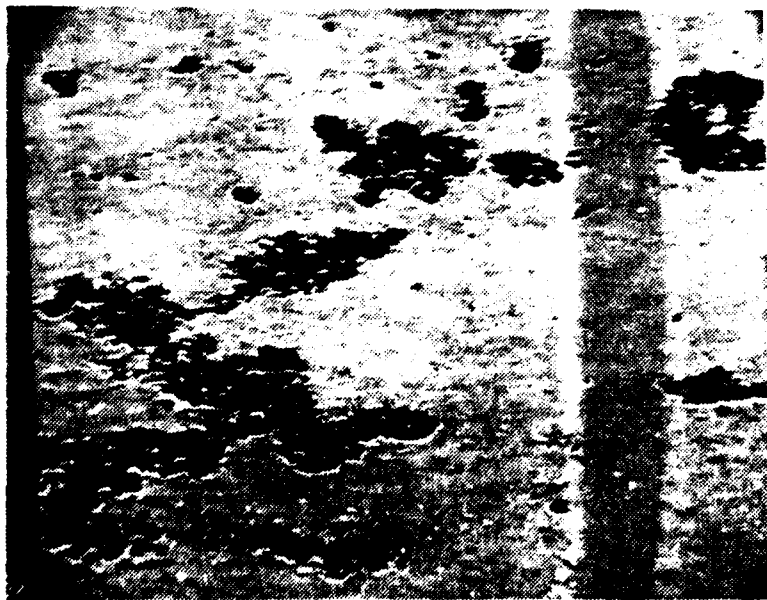

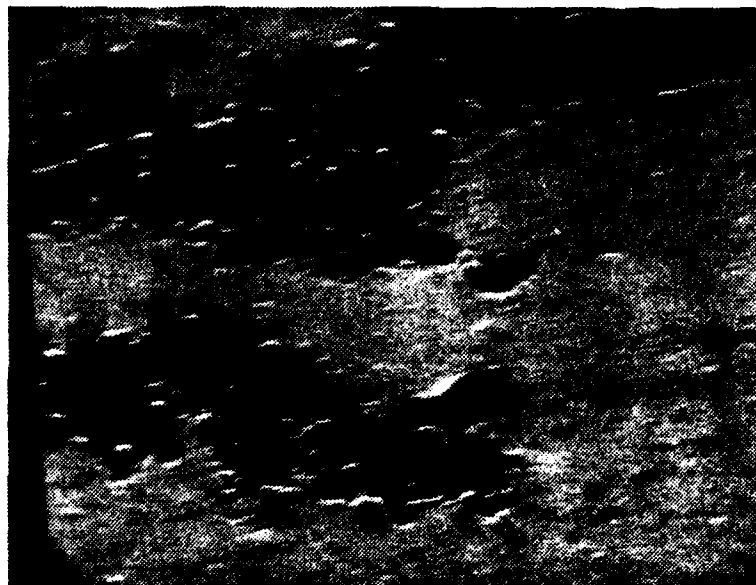FIGURE 68.   GLASS COATED WITH TITANIUM.   ENLARGED VIEW OF SMALLER ARC TRACKS.   (200X SEM)

FIGURE 69.   HIGHLY MAGNIFIED VIEW OF A SINGLE ARC TRACK.   (500X SEM)

85

2. Sample Number Two

This sample was taken from a CO_2 laser test stand. One side of the window was exposed to a plasma at atmospheric pressure. Figure 6 is a photograph of this window.

The damaged areas of the window, shown enlarged in Figure 70, consist of a central area 0.57 mm in diameter with a surrounding outer ring. The outer ring averages 1.1 mm in width. Throughout the window's surface there are widely spaced cratered areas.

Figure 71 is a magnified (40X) view of one of the damaged areas on the glass window. Streamers can be seen extending from the center of the damaged area. The streamers are probably cracks or fractures in the glass surface. The cracks could have been caused by an arc striking the glass surface. Figures 72 and 73 are an enlarged view of the damaged areas. The major damage mechanism cannot be decisively attributed to either shattering or melting. It is possible that the large globular areas were caused by melting.

a. Plasma-Surface Interaction Comments

As discussed in a previous section of this paper, any imperfection in an optical element of a laser can lead to self-focusing and damage to the element. It is conceivable that the primary damage areas seen on this sample were caused by direct laser-light pulses striking the glass surface. Since this window does not transmit the 10.6 μm CO_2 laser light, the energy would be absorbed by the glass causing damage.

86

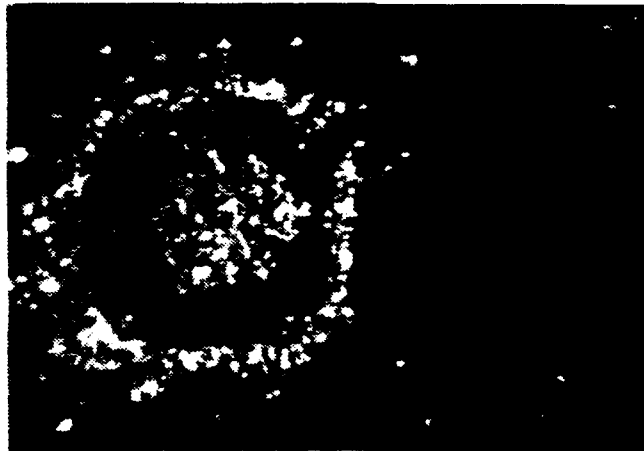FIGURE 70. MAGNIFICATION OF DAMAGED AREA ON CO_2 LASER WINDOW.

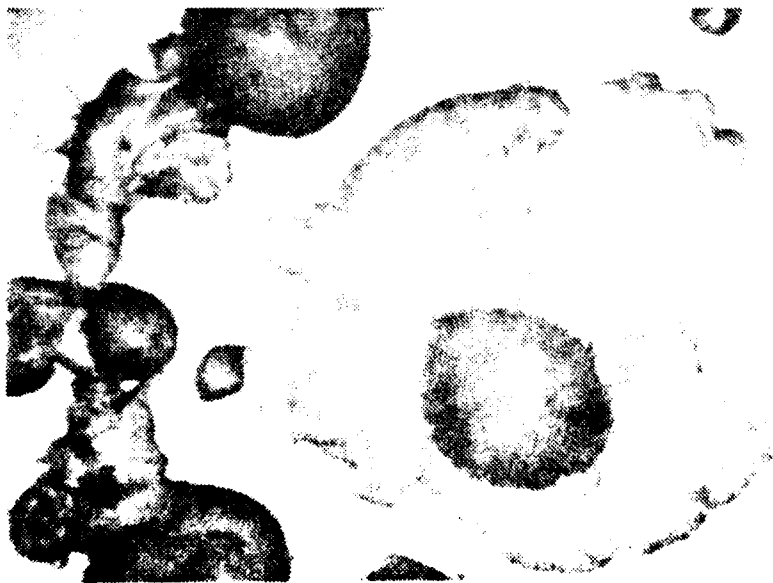FIGURE 71. DAMAGED AREA ON CO_2 LASER WINDOW. (40X OPTICAL MICROSCOPE)

FIGURE 72. DAMAGED AREA ON CO_2 LASER WINDOW. (100X OPTICAL MICROSCOPE)

88

FIGURE 73.   ENLARGED VIEW OF DAMAGE TO CO_2 LASER WINDOW.   (200X OPTICAL MICROSCOPE)

89

However, none of the available information indicates that lasing did happen.

It is possible that a speck of some conductive material or contamination was deposited on the window's surface. This would have provided a cathode-anode spot for an electrical arc between the plasma and the glass surface.

Either a laser-surface interaction or an arc could explain the unusual damage pattern. Both damaged areas consisted of a central damaged area surrounded by a seemingly undamaged area and then an outer ring of damage.

As seen in the previous samples, a plasma cloud forms an area of crater damage. If this cloud is the result of a laser interaction, the damage extends for a finite distance around the laser impact point. In this sample, however, there were two widely separated damage areas. There were no general arc craters across the surface of the sample as would be expected if a plasma cloud had reacted with the entire surface. Therefore, it is likely that this damage resulted from some localized phenomena.

3. Sample Number Three

Sample number three was a piece of titanium coated glass tubing. The titanium was applied to the tube using a plasma deposition process. This tube is shown in Figure 7. Although the coating process was done in one step, half of the coating is colored light grey and the other half of the coating is black. The grey half of the tube was directly

90

underneath and facing the titanium ball which was used as the coating source. The black half of the glass tube was further away from the titanium ball.

Figures 74 to 76 are photographs of the black coating. Each of these photographs shows arc tracks that are similar to the tracks that were observed on glass sample number one. These tracks, averaging 3 μm in width, are linked together to form a lace-like pattern. The bright areas in the pictures are bits of debris on the sample's surface. Figure 76 shows linked arc craters that form a chain.

The grey half of the tube is shown in Figures 77 to 80. This part of the tube seems to be coated with a fine powder. The imperfections on the surface appear to be raised areas rather than depressed cratered areas. Figure 79 was taken near the sample's edge. The light grey area at the bottom right of the picture is a patch of metallic glue that was used to hold the SEM sample. A bright piece of debris is in the photograph's center. Branched, river-like patterns are at the photograph's right. A magnified view of these river patterns, Figure 80, does not distinctly show whether or not these river patterns were caused by arcing. It is possible that arcing formed the river patterns and then the craters were covered with a layer of titanium.

a. Plasma-Surface Interaction Comments

Two different colored coatings were deposited upon this tube by the same plasma deposition process during the

91
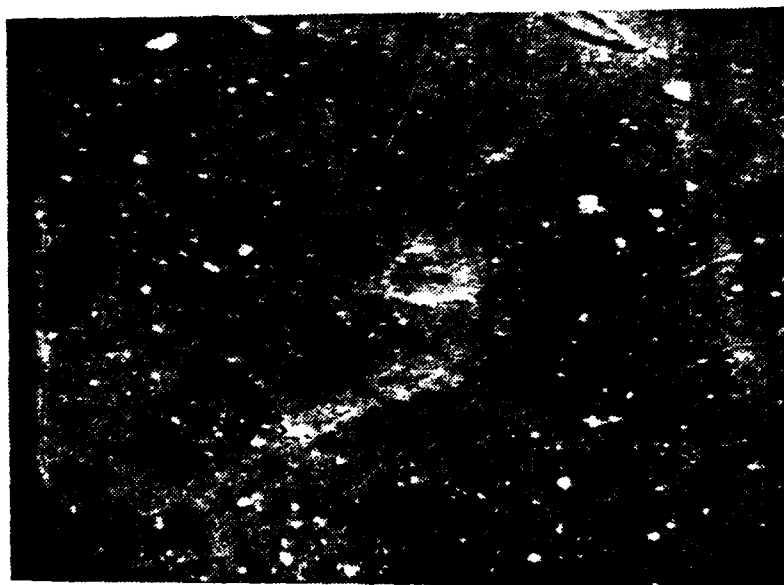
FIGURE 74. PHOTOGRAPH OF BLACK TITANIUM COATING ON GLASS. (200X SEM)
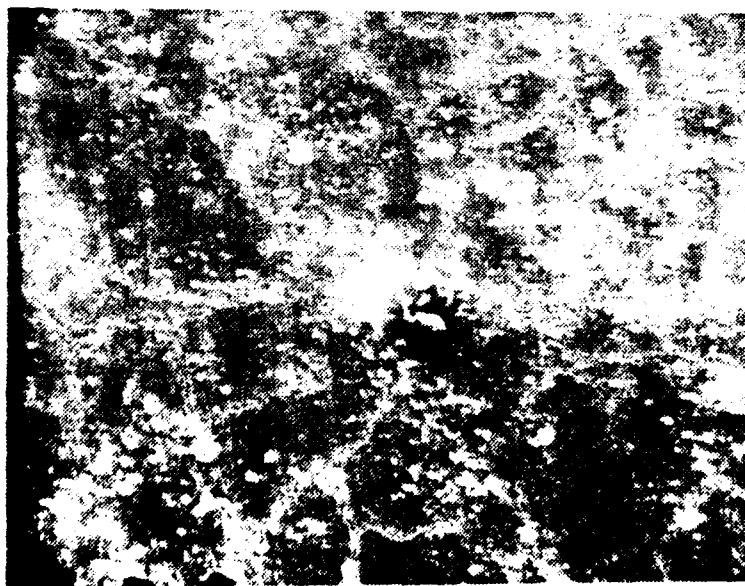
FIGURE 75. PHOTOGRAPH OF BLACK TITANIUM COATING ON GLASS. (200X SEM)
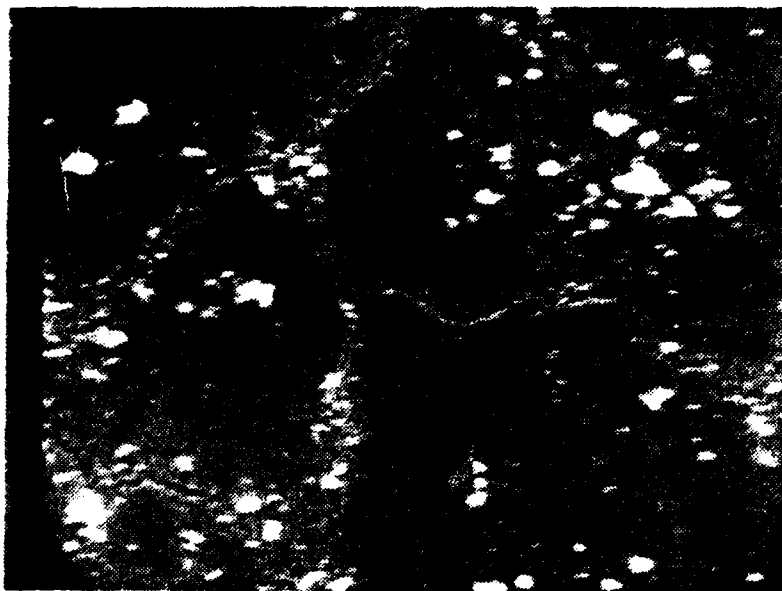
FIGURE 76. GLASS COATED WITH TITANIUM SHOWING LINKED ARC CRATERS. (500X SEM)

FIGURE 77. GLASS COATED WITH TITANIUM SHOWING GREY CLORED SECTION OF THE SAMPLE. (200X SEM)
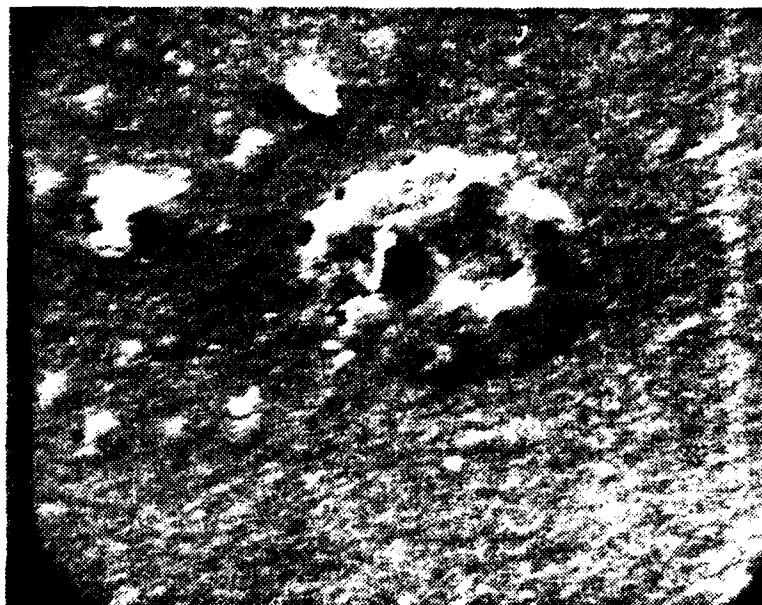
FIGURE 78.   GLASS COATED WITH TITANIUM SHOWING GREY COLORED SECTION OF
THE SAMPLE.   (500X SEM)

FIGURE 79.   GLASS COATED WITH TITANIUM SHOWING GREY COLORED SECTION F THE
SMAPLE.   THE BRIGHT SPOT AT THE CENTER IS DEBRIS.   THE GREY
AREA AT THE LOWER RIGHT IS GLUE.   (20X SEM)

FIGURE 80.   GLASS COATED WITH TITANIUM SHOWING THE GREY COLORED SECTION
OF THE SAMPLE.   (100X SEM)
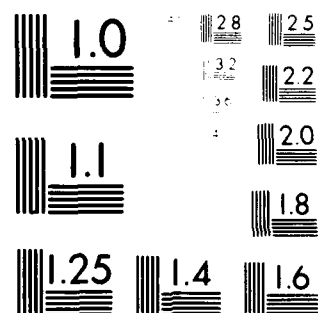
MICROCOPY RESOLUTION TEST CHART

same application. The only known difference between the black and grey areas during the deposition process was their distance to the titanium ball coating source. It is believed that the difference in the colors is attributable to a difference in their microcrystal structure. The titanium takes on a greyish color when the microcrystals formed are relatively large. The titanium shows a black appearance when formed from smaller crystals.

V. CONCLUSIONS

The study undertaken by this thesis clearly showed that plasma-surface interactions cause severe damage to many conducting materials. The primary damage mechanism in almost all cases was unipolar arcing. The name, "unipolar arcing," implies that the same surface acts as both the cathode and anode, thus completing an electrical circuit between the plasma and the material surface.

In one part of the experiment, a neodymium laser was used to induce a plasma by irradiating a target surface area of about 1 mm. Upon formation, the plasma rapidly expands radially over the target's surface and upward toward the light source. The laser energy is absorbed by the plasma, heating the plasma to sufficient temperatures to cause unipolar arcing and melting of the target out to a finite distance (about 1.8 mm in diameter in this research). Beyond this distance, plasma-surface interactions still continue in the form of unipolar arcing as long as a plasma of sufficient electron temperature and electron density is present.

The above phenomenon was expected with the plasma formed in a vacuum. Though some local surface melting was expected with the plasma formed in air at atmospheric pressure, no unipolar arcing was expected. It was thought that the laser energy would be expended ionizing the atmospheric atoms due

to the formation of a laser supported detonation wave, moving away from the target surface. This leaves insufficient laser energy to create the necessary electron temperatures and plasma electron density for unipolar arcing. This, however, was not the case. Evidence of unipolar arcing was found on all targets irradiated at atmospheric pressure that also arced in vacuum. Additionally, the extent of the total surface damage in air was not significantly different in all samples studied from the total surface damage done in vacuum. Therefore, the idea that plasma-surface interaction damage from a laser induced plasma would be much more extensive when done in a vacuum than at atmospheric pressure, could not be supported from this study.

Nickel showed much less evidence of arcing damage than the other metallic conductors. This is not understood, since nickel has the same general properties as the other metals that were tested. This is an area that requires further investigation.

Titanium is used as a coating on the components of some plasma devices, such as tokamaks, to act as an O_2 getter. While the titanium may be a good getter, it appears that it may not be suitable for the plasma environment. The titanium coatings of various materials tested in this study, were all severely damaged from unipolar arcing. The arcing leads to increased vaporization of metal atoms which undesirably pollutes the plasma. Since the arc craters erode the titanium from the surface of the components, this possibly also reduces

the effectiveness of the titanium as a getter. The gettered
oxygen will be released together with the titanium.

The samples that were exposed to a plasma in the tokamak,
had arcing craters in their titanium coatings. In most cases,
these craters linked together to form a distinct track in a
specific direction. In the case where no distinct track was
formed, it is believed that craters would have joined together
to form a track, given more exposure time. The arcing tracks
were formed in the $-(\vec{j} \times \vec{B})$ direction, where $\vec{j}$ is the arc
current density in the normal direction to the surface and $\vec{B}$
is the magnetic induction in the toroidal direction in the
tokamak.

It could not be determined if the substrate of the titanium
coated insulators were damaged by the plasma-surface interactions.
It is believed that the insulators, themselves, would not inter-
act with the plasma to form arcs. The electrical circuit could
not be completed to cause the arcs. It is conceivable, though,
that the substrate surface could be damaged by the plasma arc
after burning through the coating and heating the unprotected
substrate, causing thermal damage.

The glass window, from the Air Force laser test stand, had
an unusual damage pattern. What caused the damage is not known.
The pattern of having a circular damaged area, surrounded by a
undamaged region, surrounded by a ring of damage, was different
from any other patterns observed during this study.

This study has shown that many different metal conductors are subject to damage from plasma-surface interactions in a plasma environment. As with many technical studies, though several sought conclusions are reached, many new questions are also raised. Some of these major issues will be addressed as recommendations.

VI. <u>RECOMMENDATIONS</u>

The results of this thesis suggest many areas for further study. The metals were polished to smooth the surfaces, since surface projections and other surface irregularities enhance unipolar arcing. The degree of smoothness was not measured, however. This parameter may be an important factor in the extent of unipolar arcing damage. A study of the effect of this parameter on unipolar arcing is recommended.

In this research the samples studied were either tested in the tokamak plasma or in a laser induced plasma. No material was tested in both environments. It would be interesting to take two similarly prepared samples of the same material and expose one to the laser induced plasma and the other to the tokamak plasma. This could help develop an understanding of how closely related the induced plasma environment is to the natural plasma environments of plasma devices.

This thesis showed that there was less plasma damage at higher pressures for stainless steel. However, no significant difference was observed for copper or nickel samples tested in atmospheric pressure and vacuum. The effect of differing pressures and differing gases on unipolar arcing could be systematically investigated.

Nickel did not show the extensive signs of unipolar arcing damage from the laser induced plasma as did the other metal conductors. This phenomenon should be investigated further, since no particular parameter could be identified that could cause the difference.

The uncoated glass window from the Air Force laser test stand has an unusual damage pattern that is not understood. It may be profitable to investigate the cause of the damage to the window.

It is believed that non-conductors will not induce unipolar arcing in a plasma environment. Nothing can be concluded from this study to support or disprove this idea. All non-conductors studied were coated with titanium. Even though the coatings arced, it could not be determined if the non-conductor itself was involved in the arcing process. It is recommended that uncoated glass of a known content be exposed to a plasma to search for evidence of any arcing.

Finally, since titanium receives such severe damage when exposed to a plasma environment, its usefulness as a getter in plasma devices is jeopardized. A study to find other getters that will not arc as heavily is recommended. Another possible option is to search for a treatment that can be done to titanium to preserve its properties as a getter and greatly increase its resistance to unipolar arcing.

LIST OF REFERENCES

1. Keville, M. T. and Lautrup, R. W., _An Investigation of Unipolar Arcing Damage On Stainless Steel and Titanium Carbide Coated Surfaces_, M.S. Thesis, Naval Postgraduate School, Monterey, California, 1980.

2. Naval Research Laboratory Report 7728, _Response of Materials to Laser Radiation: A Short Course_, by J. T. Schriempf, p. 11, 10 July 1974.

3. Hughes, T. P., _Plasmas and Laser Light_, p. 273, John Wiley & Sons, 1975.

4. Ibid, p. 276

5. Ibid, p. 274

6. Naval Research Laboratory Report 7728, _Response of Materials to Laser Radiation: A Short Course_, by J. T. Schriempf, p. 36, 10 July 1974.

7. Hughes, T. P., _Plasmas and Laser Light_, p. 277, John Wiley & Sons, 1975.

8. Naval Research Laboratory Report 7728, _Response of Materials to Laser Radiation: A Short Course_, by J. T. Schriempf, p. 56, 10 July 1974.

9. Chen, F. F., _Introduction to Plasma Physics_, p. 54, Plenum Press, 1974.

10. Hughes, T. P., _Plasmas and Laser Light_, p. 287, Plenum Press, 1974.

11. Keville, M. T. and Lautrup, R. W., _An Investigation of Unipolar Arcing Damage On Stainless Steel and Titanium Carbide Coated Surfaces_, M.S. Thesis, Naval Postgraduate School, Monterey, California, p. 11, 1980.

12. Ibid, p. 11

13. Ibid, p. 9

14. Chen, F. F., _Introduction to Plasma Physics_, p. 244-249, Plenum Press, 1974.

15. Glass, A. J. and Guenther, A. H., "Damage Constraints in the Design of High Energy Lasers for Fusion Applications," Laser Interactions and Related Plasma Phenomena, v. 3A, p. 253, Plenum Press, 1973.

16. Ibid, p. 160

17. Ibid, p. 165

18. Ibid, p. 165

19. Davis, L. J., Self-generated Magnetic Field Produced by Laser Bombardment of a Solid Target, M.S. Thesis, Naval Postgraduate School, Monterey, California, 1971.

20. Metals Handbook, 8th ed., v. 2, American Society for Metals, 1964.

BIBLIOGRAPHY

Behrisch, R., Surface Erosion from Plasma Material Interaction," _Journal of Nuclear Materials_, v. 85, p. 1047 - 1061, 1979.

Chen, F. F., _Introduction to Plasma Physics_, p. 2 - 54, Plenum Press, 1974.

Culham Laboratory (UKAE) Report CLM-P 573, "Plasma-Surface Interactions in Tokamaks," by G. M. McCracken and P. E. Scott, 1979.

Davis, L. J., _Magnetic Field Produced by Laser Bombardment of a Solid Target_, M.S. Thesis, Naval Postgraduate School, Monterey, California, 1971.

Dyer, P. E., and others, "Interaction of High Power CO_2 Lasers with Solid Targets," _Laser Interactions and Related Plasma Phenomena_, v. 3A, p. 191 - 212, Plenum Press, 1973.

Glass, A. J. and Guenther, A. H., "Damage Constraints in the Design of High Energy Lasers for Fusion Applications," _Laser Interactions and Related Plasma Phenomena_, v. 3A, p. 149 - 169, Plenum Press, 1973.

Hughes, T. P., _Plasmas and Laser Light_, p. 273 - 444, John Wiley & Sons, 1975.

Hwang, Z. W., _Laser Induced Evaporation from Stainless Steel Surfaces_, M.S. Thesis, Naval Postgraduate School, Monterey, California, 1978.

Johnson, C. B., _Induced Evaporation of Metal from an Aluminum Surface by a Normal Pulse Neodymium Laser_, M.S. Thesis, Naval Postgraduate School, Monterey, California, 1979.

Keville, M. T. and Lautrup, R. W., _An Investigation of Unipolar Arcing Damage On Stainless Steel and Titanium Carbide Coated Surfaces_, M.S. Thesis, Naval Postgraduate School, Monterey, Calfornia, 1980.

Metals Handbook, 8th ed., v. 2, American Society for Metals, 1964.

Miley, G. H., Plasma Surface Arcing in Fusion Devices,
paper presented at International Conference on Plasma
Science, Montreal, Canada, 4 - 6 June 1979.

Naval Research Laboratory Report 7728, Response of
Materials to Laser Radiation: A Short Course, by
J. T. Schriempf, 10 July 1974.

Ready, J. F., "Effects Due to Absorption of Laser
Radiation." Journal of Applied Physics, v. 36,
p. 462, 1965.

Schwarz, H. J. and Hora, H., Laser Interaction and
Related Plasma Phenomena, v. 3A, Plenum Press, 1973.

S4 - 10 Stereo Scanning Electron Microscope Manual,
TL 116 - OM - 96118-002, Cambridge Scientific
Instruments Limited.

INITIAL DISTRIBUTION LIST

No. Copies

1. Defense Technical Information Center   2
   Cameron Station
   Alexandria, Virgina 22314

2. Library, Code 0142   2
   Naval Postgraduate School
   Monterey, California 93940

3. Department Chairman, Code 61   1
   Department of Physics and Chemistry
   Naval Postgraduate School
   Monterey, California 93940

4. Department Chairman, Code 69   1
   Department of Mechanical Engineering
   Naval Postgraduate School
   Monterey, California 93940

5. Assoc. Professor F. R. Schwirzke, Code 61sw   2
   Department of Physics and Chemistry
   Naval Postgraduate School
   Monterey, California 93940

6. Assoc. Professor K. D. Challenger, Code 69   1
   Department of Mechanical Engineering
   Naval Postgraduate School
   Monterey, California 93940

7. LCDR Joseph Henry Barker III, USN   2
   616 Noriega Street
   San Francisco, California 94122

8. LCDR Robert J. Rush, USN   2
   800 Faulkner Lane
   Waco, Texas 76704

107